University of Zurich[UZH]

UNIVERSITÄT BERN

Institute of Veterinary Pharmacology and Toxicology, Vetsuisse Faculty Zürich

The effect of persistent DNA damage on cancer-associated stroma

Masterthesis
Inglin Larissa

Carried out under supervision of
Dr. Markkanen Enni
Clementi Elena

Zurich, 25. January 2019

Table of Contents

1 Zusammenfassung

Wachstum und Metastasierung von Krebszellen werden stark durch das umgebende Krebs-assoziierte Stroma (CAS) beeinflusst. Eine wichtige zelluläre Komponente dieses CAS sind die sogenannten Krebs-assoziierten Fibroblasten (CAFs). CAFs fördern sowohl Wachstum als auch Metastasierung von Tumoren, und sind deshalb interessante Zielstrukturen für therapeutische Ansatzpunkte. Entzündungsmediatoren wie transforming growth factor β (TGF β), und/oder reaktive Sauerstoffradikale (ROS) können die Aktivierung von CAFs induzieren. Jedoch sind der exakte Mechanismus zur Entstehung von CAFs sowie deren Effekte auf die Tumorzellen noch nicht komplett verstanden. Die Basen-exzisions Reparatur (BER) ist ein DNA Reparaturmechanismus, welcher für den Erhalt der zellulären Genomintegrität von höchster Relevanz ist. Eine Depletion des zentralen BER Proteins XRCC1 durch knockdown (KD) führt zu persistierenden DNA Schäden, welche Genexpressions-Veränderungen induzieren die vergleichbar sind mit denen in Tumorzellen. Wir haben kürzlich gezeigt, dass TGF β und ROS in Fibroblasten persistierende DNA Schäden durch Herunterregulierung von XRCC1 hervorrufen. Dies führt wiederum zu einer Aktivierung von CAFs, welche *in vitro* Wachstum und Motilität von Tumorzellen unterstützen. Diese Umprogrammierung ist weitgehend vom Stress-induzierten Transkriptionsfaktor ATF4 abhängig, und scheint metabolische Veränderungen zu verursachen, welche möglicherweise die zelluläre Nährstoff-Selbstversorgung verbessert. Jedoch ist der Zweck dieser Umprogrammierung durch Herunterregulierung von XRCC1 noch völlig unklar. Des Weiteren haben wir gezeigt, dass ein stromaler XRCC1 KO *in vivo* verstärktes Tumorwachstum und –Metastasierung auslöst. Basierend auf diesen Ergebnissen war das Ziel dieses Projektes die Untersuchung der folgenden zwei Hauptfragestellungen:

1. Führen die XRCC1 KD-induzierten metabolischen Veränderungen zu einem Überlebensvorteil bei eingeschränkter Nährstoffversorgung? Und wenn ja, ist dies abhängig von ATF4?
2. Welche molekularen Veränderungen geschehen im CAS von XRCC1 KO Mäusen? Wie Unterstützen diese Veränderungen Tumorwachstum und Metastasierung?

Um zu untersuchen, ob die XRCC1 KD-induzierten metabolischen Veränderungen in einem Vorteil bei eingeschränkter Nährstoffversorgung resultieren, wurden die Zellen in unterschiedlichen Serum (FCS)-konditionen kultiviert. Während keine Unterschiede bei 5% FCS zu verzeichnen waren, hatten XRCC1 KD Zellen einen klaren Wachstums- und/oder Überlebensvorteil bei 1% FCS. Dieser war abhängig von ATF4. Da die Zellproliferation von XRCC1 KD Zellen sich hierbei nicht von der Kontrolle unterschied, ist die höhere Zellzahl bei 1% FCS höchstwahrscheinlich das Resultat erhöhter Resistenz gegenüber Apoptose.

Um XRCC1 KO-induzierte stromale Genexpressionsveränderungen zu identifizieren, wurde RNA von CAS und normalem Stroma mittels Laser-Mikrodissektion gefrorener Tumoren unseres Mausmodells extrahiert. Next-generation Sequenzierung enthüllte klare Unterschiede in CAS und normalem Stroma von XRCC1 KO verglichen mit Kontrollmäusen, welche möglicherweise das erhöhte Tumorwachstum und die Metastasierung erklären können.

Zusammenfassend zeigen wir, dass ein Mangel an XRCC1 zum Überleben von CAFs bei eingeschränkter Nährstoffversorgung *in vitro* beiträgt, und identifizieren molekulare Veränderungen, die möglicherweise zu Tumorwachstum und Metastasierung *in vivo* beisteuern. Verbessertes Verständnis der Umprogrammierung von CAFs und deren Effekte auf Tumorzellen trägt zum vertieften Verständnis der Grundlagenbiologie von Krebserkrankungen bei, und hat das Potenzial neuartige therapeutische Strategien zu enthüllen.

2 Summary

Cancer growth and metastasis is strongly influenced by the surrounding cancer-associated stroma (CAS). A prominent cellular component of CAS are the so-called cancer-associated fibroblasts (CAFs) which strongly support tumour growth and metastasis, and thus present an interesting target for therapeutic intervention. It is known that inflammatory cytokines, such as transforming growth factor β (TGF β) and/or reactive oxygen species (ROS) can induce activation of CAFs. However, the exact mechanism by which CAFs are induced and the effects they exert on tumour cells remain far from being completely understood. Base excision repair (BER) is a centrally important DNA repair mechanism in cells responsible for the maintenance of genome integrity. Depletion of the core BER protein XRCC1 by knockdown (KD) leads to persistent DNA damage, which induces gene-expression changes comparable to those found in tumours. We have recently found that TGF β and ROS induce persistent DNA damage in fibroblasts through down-regulation of XRCC1, which leads to activation of CAFs that support growth and motility of tumour cells *in vitro*. This reprogramming is largely dependent on the stress-responsive transcription factor ATF4, and seems to induce a metabolic rewiring that might increase nutritional self-sufficiency. However, the rationale for this reprogramming through XRCC1 downregulation remains enigmatic. Furthermore, we have discovered that a stromal XRCC1 knockout (KO) triggers increased tumour growth and metastasis *in vivo*. Based on these findings, the aim of this project was to investigate the following two main questions:

1. Do the XRCC1 KD induced metabolic changes in fibroblasts promote survival in conditions of restricted nutrient supply? If yes, is this dependent on ATF4?
2. What molecular changes can be observed in CAS of XRCC1 KO mice? How do these changes support tumour growth and metastasis?

To investigate whether the XRCC1 KD-mediated metabolic rewiring resulted in an advantage under nutrient-restricted conditions, cells were grown in different serum (FCS)-restricted conditions. While no differences were found in cells grown at 5% FCS, XRCC1 KD conferred a very clear growth and/or survival advantage at 1% FCS. This advantage was dependent on ATF4. As cell proliferation in XRCC1 KD cells did not differ from control cells, the higher cell number at 1% FCS is likely due to an increased cellular resistance to apoptosis.

To identify XRCC1 KO-induced stromal gene expression changes, we extracted RNA from CAS and normal stroma from fresh-frozen tumours derived from our mouse model using laser-capture microdissection. Next-generation sequencing revealed clear differences in CAS and normal stroma from XRCC1-KO compared to control mice, which could possibly explain the increase of tumour growth and metastasis that were observed.

In summary, we demonstrate that an XRCC1 deficiency contributes to increased survival of CAFs under nutrient-restricted conditions *in vitro*, and identify molecular changes that possibly promote tumour growth and metastasis *in vivo*. Better understanding of the reprogramming and the effects of CAFs will further our understanding of basic tumour biology and have the potential to unveil novel therapeutic strategies.

3 Abbreviations

AP site	abasic site
APE1	AP-endonuclease 1
ATF4	activating transcription factor 4
BER	base excision repair
CAF	cancer-associated fibroblasts
CAS	cancer-associated stroma
FCS	fetal calf serum
ISR	integrative stress response
KD	knockdown
KO	knockout
LCM	laser-capture microdissection
Lig III	DNA ligase IIIa
LLC	Lewis Lung Carcinoma
NGS	next-generation sequencing
OCT	optimal cutting temperature compound
Pol β	DNA polymerase β
RIN	RNA integrity number
ROS	reactive oxygen species
RT-qPCR	quantitative real-time PCR
SSB	single strand break
TGFβ	transforming growth factor β
XRCC1	X-ray repair cross complementing 1

4 Introduction

4.1 Cancer and cancer-associated stroma

The term "cancer" stands for a large group of diseases that can occur anywhere in the body. Common to all cancers is the rapid growth of abnormal cells, which is often coupled with the ability to invade and metastasise [1]. In the 21st century, cancer is expected to rank as the leading cause of death and the most important barrier to increasing life expectancy in every country of the world [2]. 3.91 million new cases (excluding non-melanoma skin cancer) and 1.93 million deaths from cancer were estimated in 2018 in Europe alone [3]. These facts highlight the importance to better understand the driving and supporting mechanisms of cancer growth, to then develop better treatments.
Historically, cancer has been viewed as a disease only depending on the abnormally growing tumour cells themselves. However, more recent research has clearly shown, that cancer growth and metastasis is strongly influenced by the surrounding non-cancerous tissue termed cancer-associated stroma (CAS). That is why, over the past decades, there has been a growing attention for the role of CAS in cancer research [4, 5]. In general, CAS consists of the non-malignant cells and their stroma within and around a tumour [4, 6]. Among other stromal components such as immune cells, angiogenic vascular cells, and extracellular matrix, one prominent cellular component of CAS are the fibroblasts, which display an activated phenotype, resembling the one found during wound healing [6]. Unlike normal fibroblasts, these so-called cancer-associated fibroblasts (CAFs) are not quiescent and supportive cells, but instead are proliferative, migratory and highly secretory [4]. They encourage and support tumour growth, angiogenesis, inflammation and metastasis and are therefore a major factor influencing tumour outcome [7]. It is known that inflammatory cytokines, such as transforming growth factor β (TGF β), and/or reactive oxygen species (ROS) can induce the activation of CAFs from normal fibroblasts [8, 9]. However, the underlying molecular mechanisms that drive CAF formation through TGF β or ROS remain unclear.
Despite the increase in possible therapeutic options, most of the available modalities set their focus on the malignant cancer cells without considering the surrounding non-cancerous part, the CAS. Given that cancer cells do not manifest the disease alone, but strongly depend on the normal surrounding cells of CAS, addressing the CAS in its molecular details is an important and promising aspect to identify targets for the development of novel therapeutic approaches.

4.2 The link between base-excision repair and cancer-associated fibroblasts

Mutations in the DNA sequence are considered the molecular origin of the vast majority of cancers. They can occur due to DNA damage, caused by various exogenous sources. But even without exogenous influence DNA is prone to spontaneous alterations, due to its chemical reactivity in the aquatic milieu [10].
Base excision repair (BER) is a centrally important DNA repair mechanism in cells that is responsible for the maintenance of genome integrity, and the avoidance of mutagenic and cytotoxic consequences [11, 12]. It corrects small base lesions and DNA single strand breaks (SSBs), that occur due to different endogenous or exogenous mutagens or the intrinsic chemical instability of the DNA molecule [10, 12]. The entire BER process is well studied and the major players involved have been known for a long time [12]. Mechanistically, BER can be roughly subdivided into the following steps: i) once a corrupted base occurs, it is recognised and released by damage-specific DNA glycosylases. ii) The arising abasic site

(AP site) is further processed by AP-endonuclease 1 (APE1), which cleaves the DNA sugar-phosphate backbone at 5' to the AP site, thus generating a SSB. iii) This SSB is substrate to a protein complex consisting of DNA polymerase β (Pol β), XRCC1 and DNA ligase IIIa (Lig III), which catalyses the addition of the missing nucleotide and seals the DNA ends, thereby restoring a fully double-stranded DNA [10, 12]. BER is a highly coordinated process, with the scaffold protein XRCC1 as a crucial factor, due to its ability to stabilise Pol β and Lig III. Thus, cells deficient in XRCC1 display reduced DNA repair and an increase in genomic instability [10, 12, 13].

It was shown that persistent DNA damage, induced through a downregulation of XRCC1 by siRNA in human primary fibroblasts, can induce gene-expression changes that are comparable to those found in tumours [10]. Furthermore, it was found that prolonged exposure to the pro-inflammatory cytokine TGFβ or ROS causes a deficiency in BER by down-regulating XRCC1 expression in primary fibroblasts [14]. Importantly, this resulted in a decreased BER capacity and persistent DNA damage, that in turn induced normal fibroblasts to assume a CAF-like phenotype capable of supporting growth and motility of tumour cells through the secretion of soluble stimulating factors *in vitro*. This reprogramming was found to be at least partially dependent on the stress-responsive transcription factor ATF4 [10, 14]. Taken together, these results suggested that the down-regulation of BER capacity through a decrease in XRCC1 expression in fibroblasts as a generalised reaction to stressful conditions might also play a role in tumour formation *in vivo* by inducing a more pro-tumorigenic stromal environment.

Based on these findings, the Markkanen lab decided to investigate, whether persistent DNA damage in stromal fibroblasts can trigger an increase in tumour growth and metastasis *in vivo*. Importantly however, a knockout (KO) of XRCC1 in the whole mouse is embryonically lethal, presumably through accumulation of unrepaired DNA damage, which is not compatible with physiological development [15, 16]. Therefore, a mouse model in which the expression of XRCC1 could be abrogated specifically in the stromal cell compartment was developed. To this end, C57Bl6-XRCC1$^{loxP/loxP}$ mice were crossed with C57Bl6-Col1a2-CreER mice. The latter are mice in which Cre expression is specific for stromal fibroblast and induced just upon administration of Tamoxifen, which makes it possible to delay the KO of XRCC1 until after birth, so eventual complications caused by the KO during embryonic development could be further reduced. Therefore, the XRCC1$^{loxP/loxP}$ Col1a2-CreER model allows a specific deletion of XRCC1 in stromal fibroblasts in mice *post natum*. Using these mice, the growth and metastasis of luciferase labelled syngeneic tumour cells injected s.c. was analysed using a combination of IVIS *in vivo* imaging and histopathology. Yet unpublished data demonstrates that a conditional deletion of XRCC1 in fibroblasts triggers an increase in both primary tumour growth as well as metastasis *in vivo* (Clementi *et al*, unpublished data).

As mentioned above, lengthened exposure to pro-inflammatory cytokines and ROS have been identified to induce a deficiency in BER through transcriptional down-regulation of XRCC1, which in turn leads to CAF activation through this exhaustion of the BER pathway [14]. But what is the rationale of this down-regulation of XRCC1 in fibroblasts under stressful circumstances? In order to answer this question, recent results from a metabolic analysis of XRCC1-depleted primary human fibroblasts have revealed vast metabolic adjustments that cause cellular metabolism to shift towards the use of the one-carbon cycle or the pentose phosphate pathway, and away from the use of the TCA cycle (Legrand *et al*, unpublished observations). Interestingly, these changes increase cellular self-sufficiency with respect to many metabolites, such as nucleotides, amino acids and energy. Of note, this metabolic rewiring was found to depend on ATF4. ATF4 is a transcription factor tightly involved in a process termed integrative stress response (ISR) [17]. In this context, in response to a variety of different stresses, ATF4 induces the expression of a multitude of genes involved in anabolic metabolism, such as nutrient

uptake, amino acid metabolism, and anti-oxidative responses. *Per definitionem*, CAFs are located closely adjacent to the epithelial tumour-forming, rapidly dividing cancer cells. These cancer cells have a huge demand in a wide variety of nutrients to sustain their high proliferative rate, and they have been shown to remodel the surrounding stroma in a way that increases the delivery of such nutrients and other growth-promoting molecules [5]. Specifically, CAFs have been found to take up metabolic waste of cancer cells to produce metabolites that in turn are secreted again to feed the tumour [18]. It is thus thought that most of the 'rich' nutrients are drained away from CAFs to support tumour growth, which results in the necessity for CAFs to survive in a 'starved' environment. The observed down-regulation of BER capacity in fibroblasts exposed to a maintained pro-inflammatory stimulation that induces CAF generation seems to thus increase self-sufficiency of these cells, which would be beneficial in a starved environment. In summary, emerging evidence strongly suggests that CAF activation through prolonged pro-inflammatory stimulation results in a BER decline. Similarly, CAF activation can be achieved simply through depletion of BER capacity through down-regulation of XRCC1. Finally, the decline in BER capacity results in an ATF4-mediated vast metabolic reprogramming which in turn seem to support nutritional self-sufficiency of CAFs.

4.3 Specific analysis of cancer-associated stroma through laser-capture microdissection and analysis by next-generation sequencing

To specifically analyse CAS from clinical tumour samples, we have recently established isolation of CAS and matched normal stroma from tumour specimen by laser-capture microdissection (LCM) coupled with next-generation sequencing (NGS) [19, 20]. LCM is a technique that allows selective isolation of microscopic areas of interest from tissue sections [21]. The tissue subsections that were isolated can then be further used to extract macromolecules, such as RNA, to interrogate the underlying molecular events, for instance through NGS. NGS is a highly valuable method that allows high-throughput analysis of gene expression patterns in samples of interest in large detail. Thus, LCM coupled with NGS allows the detailed analysis of areas of interest from animal and human tissue sections.

4.4 Aims of the project

Recent progress has started to unveil the importance of CAFs in the formation and progression of cancer. However, the exact mechanism, by which CAFs are induced and the effects they exert on tumour cells remain far from being completely understood. We have recently found that persistent DNA damage brought about through either pro-inflammatory cytokines or the depletion of XRCC1 in fibroblasts leads to the emergence of a CAF-like phenotype *in vitro*. This reprogramming is largely dependent on ATF4, and seems to induce a metabolic rewiring that promotes nutritional self-sufficiency of these cells. Furthermore, we have discovered that stromal XRCC1 deletion triggers an increase of tumour growth and metastasis *in vivo*. Based on these findings, the aim of this project was to investigate the following two main questions:

1. Does XRCC1 depletion in fibroblasts induce changes that support their survival in restricted growth conditions? If yes, is this dependent on the stress-responsive transcription factor ATF4?

2. What molecular changes can be observed in the tumour stroma of mice with a stromal XRCC1 depletion? How do these changes support tumour growth and metastasis?

In summary, the main aims of this project were to unveil how an XRCC1 deficiency contributes to growth and survival of CAFs *in vitro*, and to shed light on how it promotes tumour growth and metastasis *in vivo*. Better understanding of the reprogramming and the effects of CAFs will further our understanding of basic tumour biology and have the potential to unveil novel therapeutic strategies.

5 Material and Methods

5.1 Analysis of cancer-associated stroma from the mouse model

5.1.1 Cryo laser-capture microdissection

5.1.1.1 Origin of tissue

Conditional XRCC1 KO in fibroblasts – The tissue samples for this experiment came from a mouse model with fibroblast-specific KO of XRCC1 induced through a Tamoxifen-inducible Cre/loxP approach [22]. Shortly after weaning at 3 weeks *post natum*, experimental (Col1a2-Cre Tg/+, XRCC1 Tg/Tg) and control (Col1a2-Cre Tg/+, XRCC1 wt/wt or Col1a2-Cre +/+, XRCC1 Tg/Tg) male mice were fed a Tamoxifen diet (Tamoxifen Lab Animal Diet (TD.07262; 400 mg tamoxifen citrate per kg diet; Harlan Laboratories)) for 4 weeks continuously to induce the KO in the experimental mice or to control for the effect of Tamoxifen and Cre expression alone in control mice. After completion of this diet, mice were put back on standard diet for at least two weeks before starting with the injection of tumour cells.

Tumour cell injection – 1-10 x 10e6 Luciferase-labelled Lewis Lung Carcinoma (LLC) murine tumour cells in 0.15 ml PBS were implanted subcutaneously into the shaved lower back of the mice on the right side. For this procedure mice were anesthetised with isoflurane.

Tumour resection – After 3 to 4 weeks, when the primary tumours reached a size of maximally 1.5 cm diameter, the tumours were surgically resected. The excised tumours were cut in half, with one half being fresh frozen for subsequent isolation of stroma through laser-capture microdissection (as detailed below), and the other half undergoing formalin fixation for histopathological analyses

Samples of normal skin – When the mice were sacrificed under anaesthesia, around 3 weeks after the excision of the primary tumour, a small piece of skin from the back of the mouse on the side opposite of the primary tumour was excised and immediately fresh-frozen. This skin was considered as healthy, non-tumour affected stroma.

5.1.1.2 Fresh-freezing of tissue specimen

Liquid nitrogen was poured in a styrofoam container and a can filled with isopentane placed in it. The excised tissue was put in a bucket formed out of aluminium foil with a layer of optimal cutting temperature compound (OCT) (Cellpath™) at the bottom and then covered with OCT completely. The aluminium bucket with the tissue inside was then immersed into the isopentane with wooden tweezers. Before the can containing the isopentane would start to freeze, it was taken out of the liquid nitrogen with the aluminium bucket still in it. When the OCT was frozen completely (recognised through a change of colour from clear to milky) the bucket was removed, and the frozen tissue block was wrapped in aluminium foil and stored in -20°C until all samples had been collected. Afterwards, the tissue blocks were stored at -80°C until needed.

5.1.1.3 Slide preparation

Fresh frozen samples were taken out of -80°C and transported to the Institute of Veterinary Pathology Zürich on dry ice for histologic processing. The samples were mounted on OCT in a microtome-cryostat and cut to 10 µm sections. All the equipment was treated with RNAse AWAY® (Molecular BioProducts™). The sections were mounted on Arcturus® PEN Membrane Glass Slides (Applied Biosystems™), two sections per slide.
To get an overview of the tissue section for microdissection, one section was mounted on a normal glass slide and stained with H&E staining. The unstained slides were put in a box with dry ice to bring them back to the lab, where the slides were stored in a box in -80°C until microdissection. According to the Arcturus "Optimized Protocol for Preparing and Staining LCM Samples from Frozen Tissue and Extraction of High-Quality RNA" handbook, the mounted sections can be stored for up to two months in -80°C, so all the samples for the following week were cut on Monday and stored till the day they were needed, without recognisable harm.

5.1.1.4 Staining and laser-capture microdissection (LCM)

Frozen tissue sections were transported on dry ice. One slide per time was taken out and left one minute to adjust to room temperature. Then it was stained with Cresyl Fast Violet according to the following protocol (Table 1) using Cresyl violet (acetate) for microscopy Certistain® and ethanol (Honeywell Riedel-de Haën).

95% ethanol	30 sec
75% ethanol	30 sec
Cresyl violet (75% ethanol with dH2O)	40 sec
75% ethanol	30 sec
95% ethanol	30 sec
100% ethanol	30 sec
100% ethanol	30 sec
100% ethanol	5 min

Table 1: Staining protocol for fresh frozen tissue sections

The ArcturusXT™ Laser Capture Microdissection System (Thermo Scientific) and Arcturus® CapSure® Macro LCM Caps (Life Technologies) were used for microdissection according to the manufacturer's protocol.
Photographic documentation of the microdissection process was performed throughout the whole process (see Figure 1, Figure 2). To verify the specificity of the isolation procedure, both the area of interest and the isolated tissue on the cap were reviewed after excision (Figure 11 and Figure 12).

Isolation of tumour stroma – Tumour stroma for isolation was identified with the help of a pathologist. Stroma inside the tumour and within a range of 2 mm around the tumour was collected, avoiding areas with heavy inflammation, glands, hair follicles, fat and muscle cells. Since the tumours contained little stroma, three slides with two sections each were used to fill one Cap.

Isolation of normal stroma from skin – Normal stroma was collected from two slides with two sections each. Similar to the tumour samples, glands, hair follicle, fat and muscle cells were avoided as far as possible.

The caps filled with excised tissue were kept on 0.5 ml microcentrifuge tubes (Eppendorf® Safe-Lock Tubes) and put on ice until the whole procedure was finished.

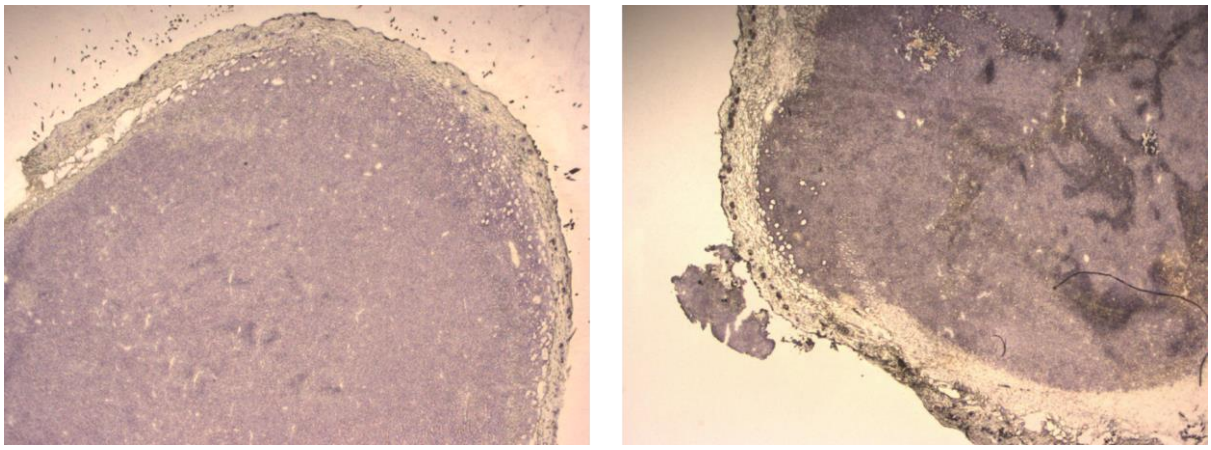

Figure 1: Example of Cresyl violet stained sections of tumour tissue at 2x magnification, right: SM6025LL (Case 3, Control), left: SM6077LL (Case 5, XRCC1 KO)

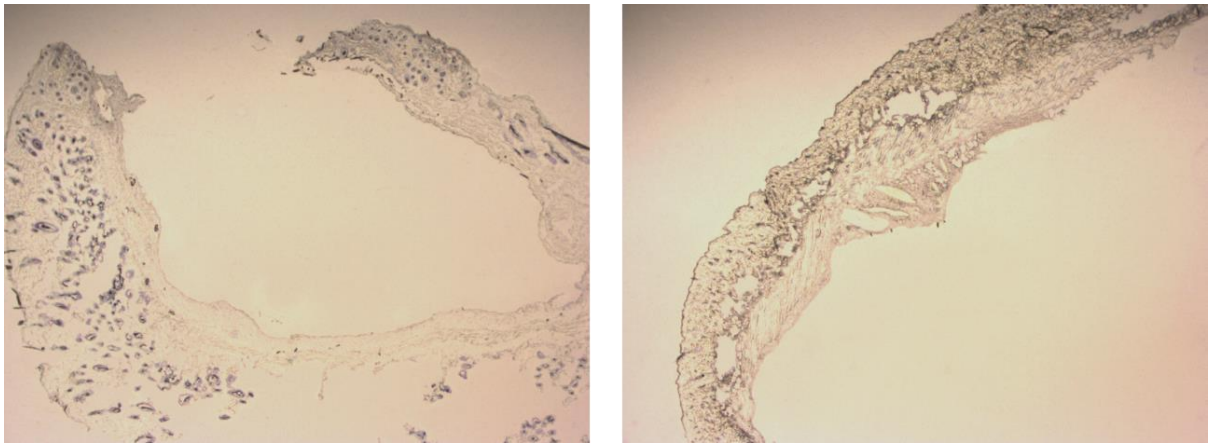

Figure 2: Example of Cresyl violet stained sections of unaffected skin at 2x magnification, right: SM6025LL (Case 8, Control), left: SM9172RR (Case 15, XRCC1 KO)

5.1.2 mRNA isolation

5.1.2.1 Extraction

mRNA extraction was done immediately after microdissection using the RNeasy® Mini Kit by QIAGEN according to the manufacturer's protocol "Purification of Total RNA from Animal Cells using Spin Technology" in the RNeasy® Mini Handbook with the following adjustments. To transfer the tissue from the caps into tubes, the thermoplastic film containing the collected tissue was peeled off the cap with a sterile blade and put in a 1.5 ml microcentrifuge tube (Eppendorf® Safe-Lock Tubes) with 110 µl of Buffer RLT.

Initially, different tissue homogenisation procedures were tested for their performance: either through varying durations of sonication with either Covaris® E220 Focused-ultrasonicator (Table 5) or Bioruptor® plus (Table 6), or just vortexing the tube without sonication. Vortexing proved to be the simplest and best protocol. Therefore, in all the following experiments tissue homogenisation was done by vortexing the tube repeatedly during 5 minutes and keeping it on ice in between. After 5 minutes, 110 µl of 70% ethanol was added and the protocol was further followed from step 5 onwards, including the on-column DNase digestion. At the end, RNA was eluted in 30 µl RNase-free water and reloaded for a second elution step. Eluted RNA was aliquoted and immediately frozen and kept at -80°C.

5.1.2.2 Quantification

For one trial experiment, Thermo Scientific™ NanoDrop™ 2000/2000c Spectrophotometer was used according manufacturer's instruction to quantify the mRNA yield (Table 6).
For all the other experiments, quantification and quality control of the extracted mRNA was done by using 2200 Tape Station Software (Agilent Technologies) according to manufacturer's instructions.

5.1.3 Next-generation RNA sequencing

10 ng of RNA diluted to a concentration of 0.33 ng/µl in a total volume of 30 µl was submitted for next-generation RNA sequencing. The SMARTer Stranded Total RNA-seq Kit—Pico Input Mammalian (Clontech/ Takara Bio USA) was used according to manufacturer's protocol for RNA library preparation and ribosomal RNA depletion. Single-read sequencing (125bp) was run using the Illumina HiSeq 4000 according to standard protocols of the Functional Genomics Centre Zurich (FGCZ). Quality control for the resulting NGS reads was performed with FastQC (http://www.bioinformatics.babraham.ac.uk/projects/fastqc). Trimmomatic [23] (v.0.36, 4 bases hard-trimming from the start, and adapter trimming at the end) was used to trim the reads and STAR [24] (version 2.6.0c) was applied to align the trimmed reads with the reference genome and transcriptome (FASTA and GTF files, respectively, Ensembl, release89, CanFam3.1). Kallisto [25] (version 0.43.1) was used for gene expression quantification. For identification of differently expressed genes the R/Bioconductor package edgeR [26] (R version: 3.5.0, EdgeR version: 3.22.1) with the implemented count based negative binominal model was applied using the normalisation factor calculated by the trimmed mean of M values (TMM) method [27].

Analysis of RNA sequencing data
Unsupervised hierarchical clustering ($p \leq 0.01$, log2 ratio threshold of 0.5) was conducted for both, comparison of tumour stroma from Con and KO animals, and normal stroma from Con and KO animals. Gene ontology (GO) enrichment analysis was performed using goseq R Bioconductor package [28].

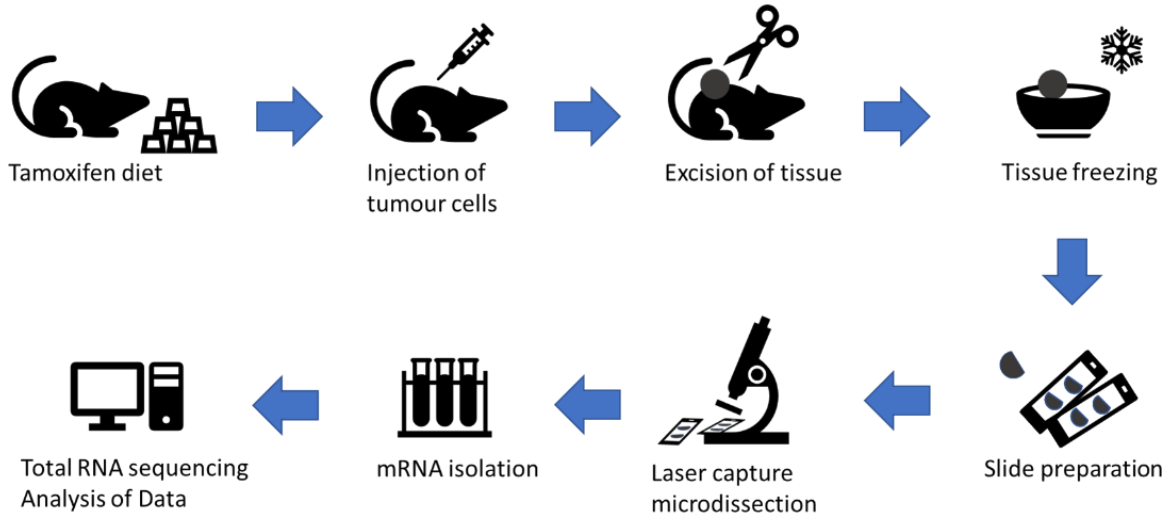

Figure 3: Overview of workflow from tissue proceeding till analysis

5.2 Analysis of TIG-1 fibroblasts cultured in different FCS conditions

5.2.1 Cell culture

TIG-1 primary human fibroblasts were purchased from Coriell and cultured under standard conditions (37°C, 5% CO2) in Gibco™ DMEM, low glucose, GlutaMAX™ Supplement, pyruvate containing 15% fetal calf serum (FCS).

5.2.2 Transfection

At day one, four 10cm diameter dishes with 800'000 cells each were seeded. For siRNA delivery Lipofectamine™ RNAiMAX Transfection Reagent (Invitrogen) was used, according to the manufacturer's protocol. Part of the experiments were performed with two different sequences of XRCC1 siRNA to exclude off-target effects. For ATF4 two siRNA sequences were used in combination to achieve an appropriate level of knockdown. As a control, an unspecific siRNA sequence that does not target any gene product was used to mimic the transfection.
Transfection was performed the day after seeding.

siRNA	Sequence	Manufacturer	Reference
siControl	Manufacturer's proprietary information	Eurogentec	Eurogentec
siXRCC1-1	5'-AGGGAAGAGGAAGUUGGAU-3'	Eurogentec	[29]
siXRCC1-2	5'-GCUUGAGUUUUGUACGGUU-3'	Eurogentec	[10]
siATF4-1	5'-GCCUAGGUCUCUUAGAUGA-3'	Eurogentec	[10]
siATF4-2	5'-CUGCUUACGUUGCCAUGAU-3'	Eurogentec	[10]

Table 2: siRNA used for transfection

5.2.3 Splitting of cells

24 hours after transfection, each of the transfected dishes was washed and trypsinised with 1 ml 1 x Trypsin solution. Trypsin was neutralised through addition of 2 ml of DMEM containing 5% FCS, and 3 ml of the solution was distributed into 3 fresh 10 cm dishes with 10 ml of medium containing different concentrations of FCS to achieve final FCS concentrations of 15%, 5% and 1%, respectively, and incubated another 48 hours until analysis (Figure 4).

5.2.4 Pictures of live cells

Three days after transfection, dishes were photographed with a phase-contrast microscope at 10x magnification, right before collecting the cells.

5.2.5 Collection of cells

The cells were collected 72h after transfection after washing once with cold 1 x PBS by scraping them off the petri dish in cold PBS. Cells were pelleted through centrifugation at 454 rcf at 4°C, and the pellets were stored in -80°C until further analysis.

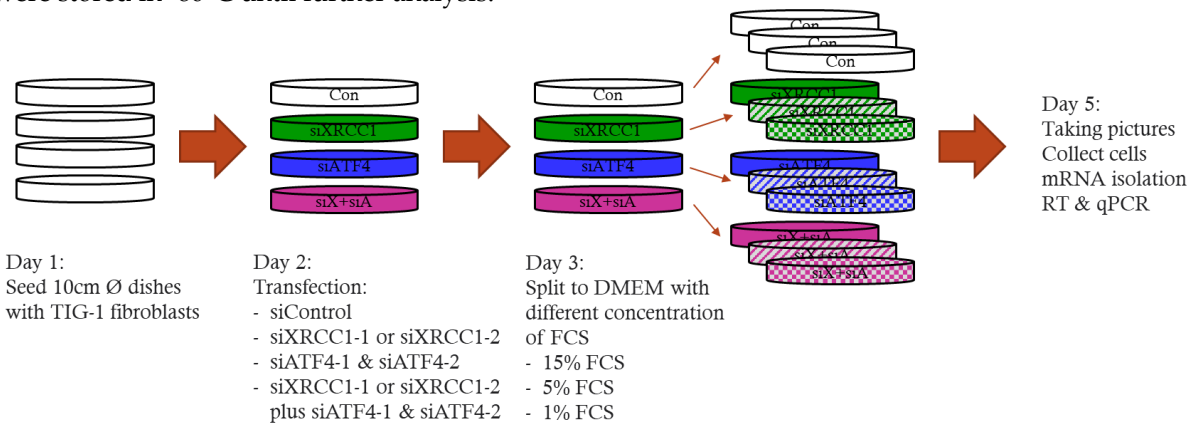

Figure 4: Scheme of general experimental setup to investigate the expression of CAF markers in TIG-1 fibroblasts grown in medium containing different concentrations of FCS.

5.2.6 Cell cycle analysis by flow cytometry

For cell cycle analysis by FACS, trypsinised cells were fixed in ice-cold 70% ethanol for at least 30 min. To remove the fixation solution, cells were spun 5 min @ 250 rcf @4°C, and the supernatant was discarded. Cells were then resuspended in phosphate buffered saline with 100 µg/ml of DNase free RNase A (Sigma) and incubated @37°C for 30 min, and further stained with 10 µg/ml propidium iodide (Sigma). Samples were run on a FACScan (BD Biosciences) and the cell cycle distribution analysed using Modfit LT software (Verity Software House).

5.2.7 mRNA isolation

5.2.7.1 Extraction

RNA extraction was performed using the RNeasy® Mini Kit by QIAGEN according to the manufacturer's protocol "Purification of Total RNA from Animal Cells using Spin Technology" in the RNeasy® Mini Handbook, starting with 350 µl of RLT buffer. Homogenisation was done as described in step 3c. To elute the RNA 30 µl of RNase-free water was used.

5.2.7.2 Quantification

Thermo Scientific™ NanoDrop™ 2000/2000c Spectrophotometer was used according manufacturer's instruction to quantify the extracted mRNA.

5.2.8 Reverse transcription

RNA was reverse transcribed using the BioRad iScript™ cDNA Synthesis Kit according to manufacturer's protocol with the LabCycler (SensoQuest), starting with 1000 ng RNA in 20 µl. The final product was diluted 1:5 in 80 µl dH2O and stored @ -80°C.

5.2.9 RT-qPCR

Quantitative real-time PCR (RT-qPCR) was done using the KAPA SYBR® FAST One-Step RT-qPCR Kit. 2 µl of each cDNA in a total volume of 10 µl was used and each sample run in duplicates on the CFX384 Touch™ Real-Time PCR detection system (BioRad). B2M and GAPDH were used as housekeeping genes. For quantification of gene expression, the comparative CT method was used, and results were expressed as fold change in mRNA levels. Primers used for RT-qPCR are detailed in Table 3.

Gene target	Sequence	Reference
XRCC1	Fw: 5'-AACACGGACAGTGAGGAACA-3' Rw: 5'-GCTGTGACGTATCGGATGAG-3'	[10]
ATF4	Fw: 5'-GGGACAGATTGGATGTTGGAGA -3' Rw: 5'-ACCCAACAGGGCATCCAAGT-3'	[10]
ACTA2	Fw: 5'-TCAATGTCCCAGCCATGTAT-3' Rw: 5'-CAGCACGATGCCAGTTGT-3'	[30]
PALLD	Fw: 5'-AACCGAGCAGGACAGAAC-3' Rw: 5'-TGGTGGCACTCCCAATAC-3'	[14]
FAP	Fw: 5'-TCAGTGTGAGTGCTCTCATTGTAT-3' Rw: 5'-GCTGTGCTTGCCTTATTGGT-3'	[14]
PSAT1	Fw: 5'-CGGTCCTGGAATACAAGGTG-3' Rw: 5'-AACCAAGCCCATGACGTAGA-3'	[10]
SPARC	Fw: 5'-GAAAGAAGATCCAGGCCCTC-3' Rw: 5'-CTTCAGACTGCCCGGAGA-3'	[14]
B2M	Fw: 5'-ATGTCTCGCTCCGTGGCCTTA-3' Rw: 5'-ATCTTGGGCTGTGACAAAGTC -3'	[14]
GAPDH	Fw: 5'-AGCCACATCGCTCAGACAC-3' Rw: 5'-GCCCAATACGACCAAATCC-3'	[10]

Table 3: List of primers used for RT-qPCR

5.2.10 Western blot

5.2.10.1 Protein extraction

For Western blot, whole cell extracts were prepared from collected TIG-1 pellets. For lysis, pellets were resuspended in M-PER™ Mammalian Protein Extraction Reagent supplemented with the cOmplete™, Mini, EDTA-free Protease Inhibitor Cocktail (Roche). The solution was kept for 30 minutes on a rotator wheel at 4°C. After the 30 minutes, the lysate was sonicated with Bioruptor® plus at 4°C, using three cycles with 30 seconds of sonication followed by a pause of 30 seconds each. At the end, the samples where centrifuged for 20 minutes at 4°C at 16049 rcf and the supernatant was transferred to a new 1.5ml tube (Eppendorf® Safe-Lock Tubes) and stored in -80°C.

5.2.10.2 Quantification of total protein content

Quantification of total protein was done using the Bradford assay right before loading the gel according to the manufacturer's specifications. All samples were measured in duplicates.

5.2.10.3 Gel preparation and Western blot

Protein samples were run on the NovexTM WedgeWellTM 4-20% Tris-Glycine Gel (Invitrogen by Thermo Fisher Scientific) with 15-wells. 20 µg of protein in a total volume of 35µl were prepared per sample, containing 7 µl of leammli loading buffer (5x) and run with PowerEase® 500 (life technologies TM) for 1 hour 30 minutes at 125V.
Transfer of proteins onto Immobilon PVDF FL membrane was performed using the novex® XCell II TM Blot Module (life technologies TM) for 2 hours at 25V.
After incubation with the primary and secondary antibodies (see Table 4), respectively, the membrane was scanned with Odyssey® CLx. Image StudioTM was used to analyse and quantify protein bands.

5.2.10.4 Antibodies for Western blot

Antibody	Manufacturer, order no.	Isotype
Palladin	Novus Biologicals, NBP1-25959	Mouse monoclonal
PSAT1	Novus Biologicals, 21020002	Rabbit polyclonal
αSMA	Dako Cytomation, M0851	Mouse monoclonal
GAPDH	Abcam, ab9484	Mouse monoclonal
Tubulin	Sigma, T5168	Mouse monoclonal

Table 4: List of antibodies used for Western blot

5.3 Statistical analysis and representation of results

GraphPad Prism was used for statistical analysis and visual representation of the collected RT-qPCR and Western blot data.

6 Results

6.1 Analysing the impact of XRCC1 depletion in TIG-1 fibroblasts under nutrient-restricted conditions

6.1.1 XRCC1 KD imparts TIG-1 cells with a growth and/or survival advantage under low-serum conditions

Yet unpublished results from metabolomics analyses of control and XRCC1 KD TIG-1 human primary fibroblasts suggested a depletion in BER capacity to induce a metabolic rewiring that promotes nutritional self-sufficiency of these cells. To investigate whether this XRCC1 KD-mediated metabolic rewiring could indeed result in better growth of TIG-1 cells under nutrient-restricted conditions, we exposed cells to culture medium containing different amounts of fetal calf serum (FCS) after siRNA treatment, and analysed cell morphology and density 72h after KD using images taken with a phase-contrast microscope (see Figure 4 for a scheme of the experiment). The respective KDs were validated by RT-qPCR (Figure 7). When cells were grown in medium containing 5% FCS, no clear differences in cell number or morphology could be observed between XRCC1 KD cells and control cells (Figure 5A and B). Interestingly however, when the FCS concentration was lowered to 1%, XRCC1 KD cells clearly displayed a vastly increased cell number, a more elongated fibroblast-like cell morphology and less rounded and floating cells compared to controls (Figure 6). These results were confirmed in several independent repetitions of the experiment (n = 4), and were also validated with a second siRNA sequence against XRCC1 (data not shown).
Taken together, our results strongly support the hypothesis that XRCC1 KD confers the cells with a selective survival and/or growth advantage in nutrient-limited conditions.

6.1.2 The XRCC1 KD-induced growth and/or survival advantage of TIG-1 cells in low-serum conditions is mediated by ATF4

Since XRCC1 KD has been shown to induce the transcription factor ATF4 in TIG-1 cells, which can induce metabolic adaptations to stressful conditions [10, 31], and our metabolomics analyses indicated the metabolic rewiring after XRCC1 KD to be largely dependent on ATF4 (unpublished observations), we wanted to investigate whether the increased growth and/or survival of TIG-1 cells upon XRCC1 KD in low FCS conditions were due to ATF4. Knocking down ATF4 alone or in combination with XRCC1 showed a slight decrease in cell numbers and slightly more floating cells at 5% FCS compared to control cells, suggesting that a baseline ATF4 level is required for optimal fitness of TIG-1 cells (Figure 5C and D). Strikingly, when cultured at 1% FCS, a combined KD of ATF4 and XRCC1 completely rescued the phenotype observed with XRCC1 KD alone, and was virtually indistinguishable from control cells (Figure 6D).
To verify that the different growth conditions did not alter KD efficiency, we analysed expression of XRCC1, ATF4 and several of their respective downstream targets by RT-qPCR in cells grown in 15%, 5%, or 1% FCS (Figure 7). KD efficiencies for XRCC1 and ATF4 were comparable in all three conditions. The effectiveness of ATF4 KD was further demonstrated by the strong decrease in expression of PSAT1, a direct downstream target of ATF4, either with ATF4 KD alone or in combination with XRCC1 KD. As reported previously [10, 14], XRCC1 KD resulted in inductions of PSAT1, ACTA2, PALLD, FAP and SPARC (Figure 7), which was also confirmed with an independent siRNA against XRCC1 (Figure 8).

Expression of PSAT1, ACTA2, and PALLD, but not of FAP and SPARC, could be rescued upon co-KD of ATF4, as expected [10, 14]. Similarly, analysis of protein expression of PALLD, ACTA2 and PSAT1 demonstrated the ATF4-dependent induction of these targets after XRCC1 KD at 5% and 1% FCS, respectively (Figure 9). Thus, varying FCS conditions did not cause differences in KD efficiency.
Summarising, these findings suggest that the survival and/or growth advantage in TIG-1 cells imparted by XRCC1 KD at low serum concentrations depends on the transcription factor ATF4.

6.1.3 The XRCC1 KD-mediated growth advantage of TIG-1 cells under low-serum conditions is not caused by increased proliferation, but likely due to an increased resistance to apoptosis

The increased cell number of XRCC1 KD cells under low FCS conditions could in principle either be due to increased proliferation or decreased apoptosis, or a combination of both. To differentiate between the two scenarios, we analysed the cell cycle distribution of control and XRCC1 KD cells grown in 1%, 5%, and 15% FCS, respectively, using flow cytometry. As expected from previous findings [10], XRCC1 KD cells grown at 15% FCS displayed an increase in G1 cells, and a concomitant decrease in S-phase cells, suggesting that XRCC1 KD under these conditions causes the cell cycle to slow down slightly by prolonging the G1-phase (Figure 10). Similarly to this, the cell cycle distribution at 5% still displayed more XRCC1 KD cells in G1 and slightly less in S-phase, compared to control cells. When analysing cells grown at 1% FCS, however, no significant differences in the percentage of cells in G1, S, or G2 cell cycle phases could be detected between control and XRCC1 KD cells. Indeed, the amount of control cells in G1 clearly increased and cells in S-phase decreased with lower FCS concentrations, while no FCS-dependent change of cell cycle distribution could be observed for XRCC1 KD cells. These findings show that XRCC1 KD do not have a proliferative advantage over control cells at low FCS conditions. Therefore, it is highly likely that the difference in cell density at low FCS concentrations is due to a lower rate of apoptosis in XRCC1 KD cells compared to control cells. This hypothesis is supported by the phenotype of control cells grown at 1% FCS that show an increase in rounded, detaching cells (Figure 6A).
In conclusion, our analyses clearly demonstrate that a KD of XRCC1 in TIG-1 cells induces a survival advantage under serum-restricted growth conditions that depends on the transcription factor ATF4, presumably through rendering cells more resistant to apoptosis.

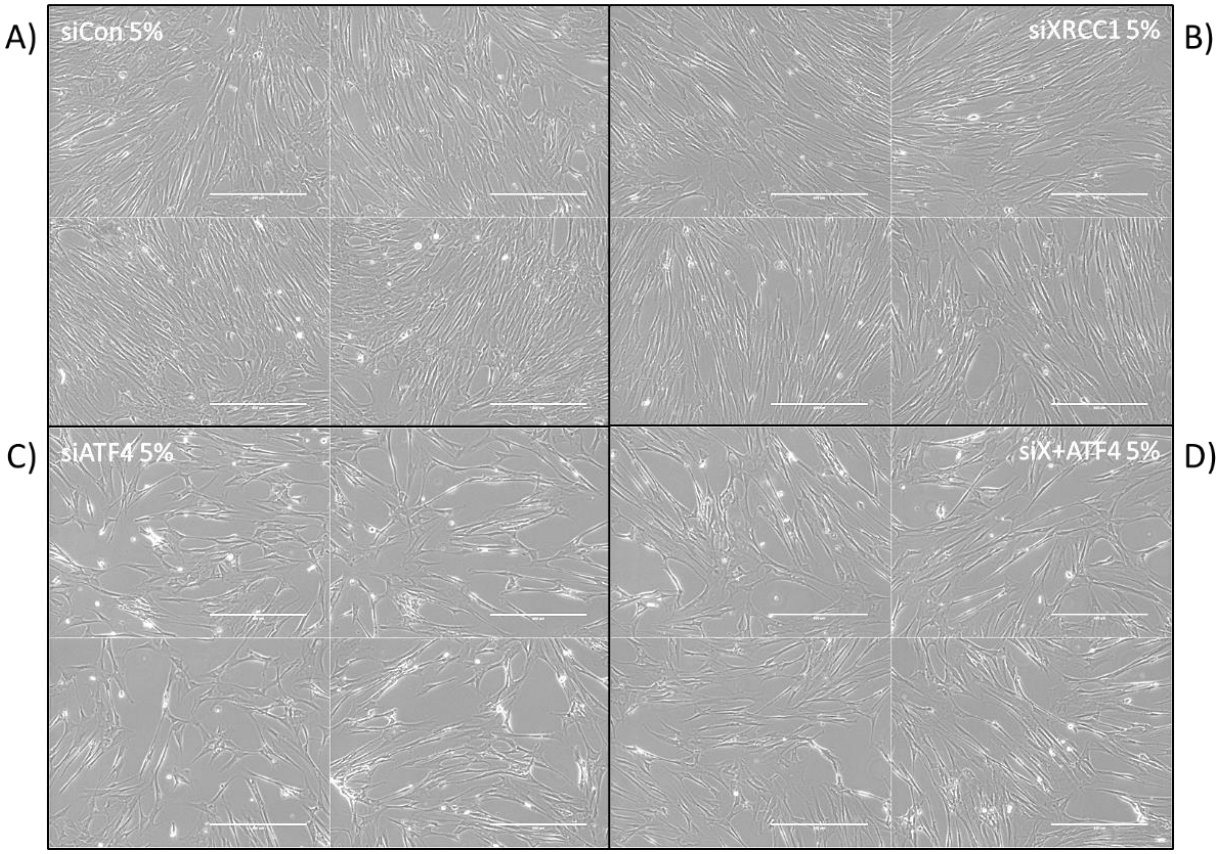

Figure 5: No difference in growth of control vs XRCC1 KD TIG-1 at 5% FCS. Phase-contrast images of TIG-1 human fibroblasts from one representative experiment taken on the third day upon transfection with siRNAs as indicated, started with the same number of cells in each condition and split to DMEM medium containing 5% of FCS 24 h after transfection. Four different fields randomly chosen on each plate are shown per condition.

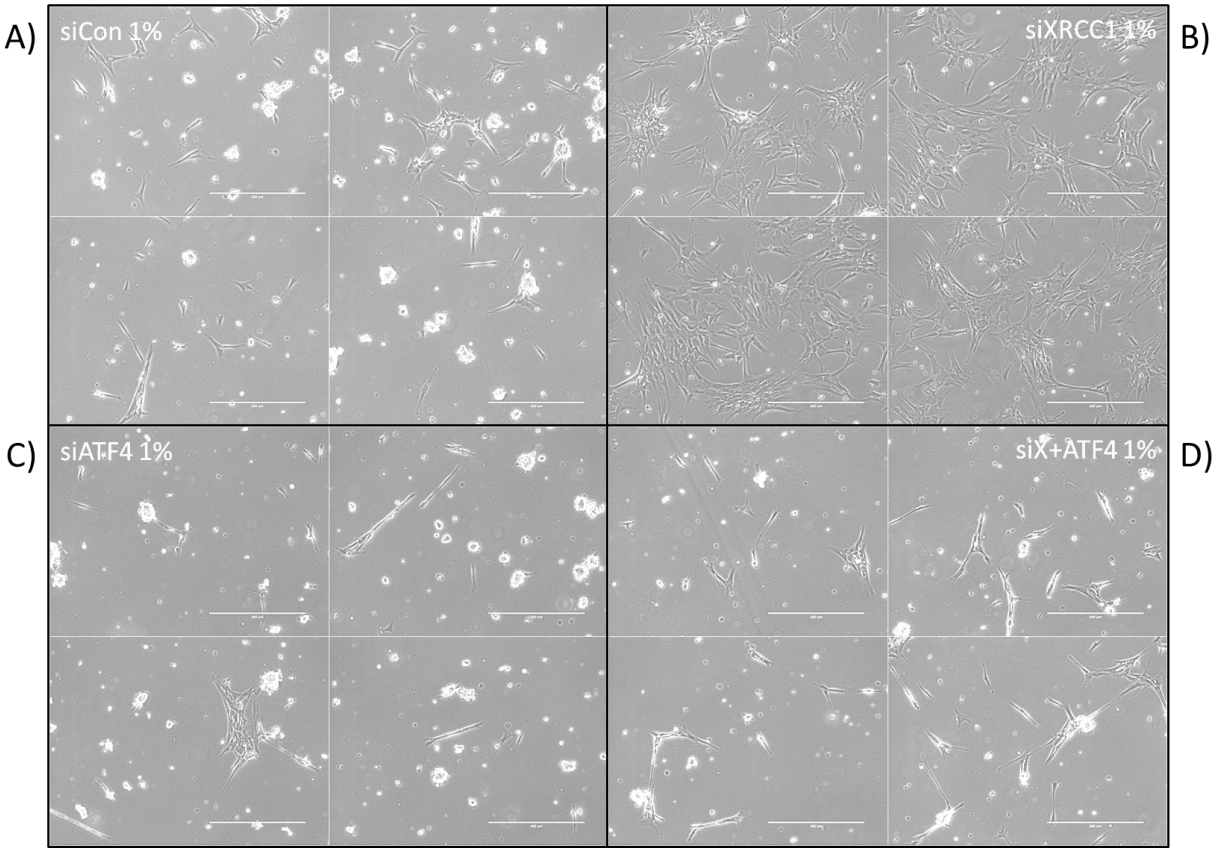

Figure 6: Selective growth and/or survival advantage of XRCC1 KD TIG-1 cells at 1% FCS. Phase-contrast images of TIG-1 human fibroblasts from one representative experiment taken on the third day upon transfection with siRNA as indicated, started with the same number of cells in each condition and split to DMEM medium containing 1% of FCS 24 h after transfection. Four different fields randomly chosen on each plate are shown per condition.

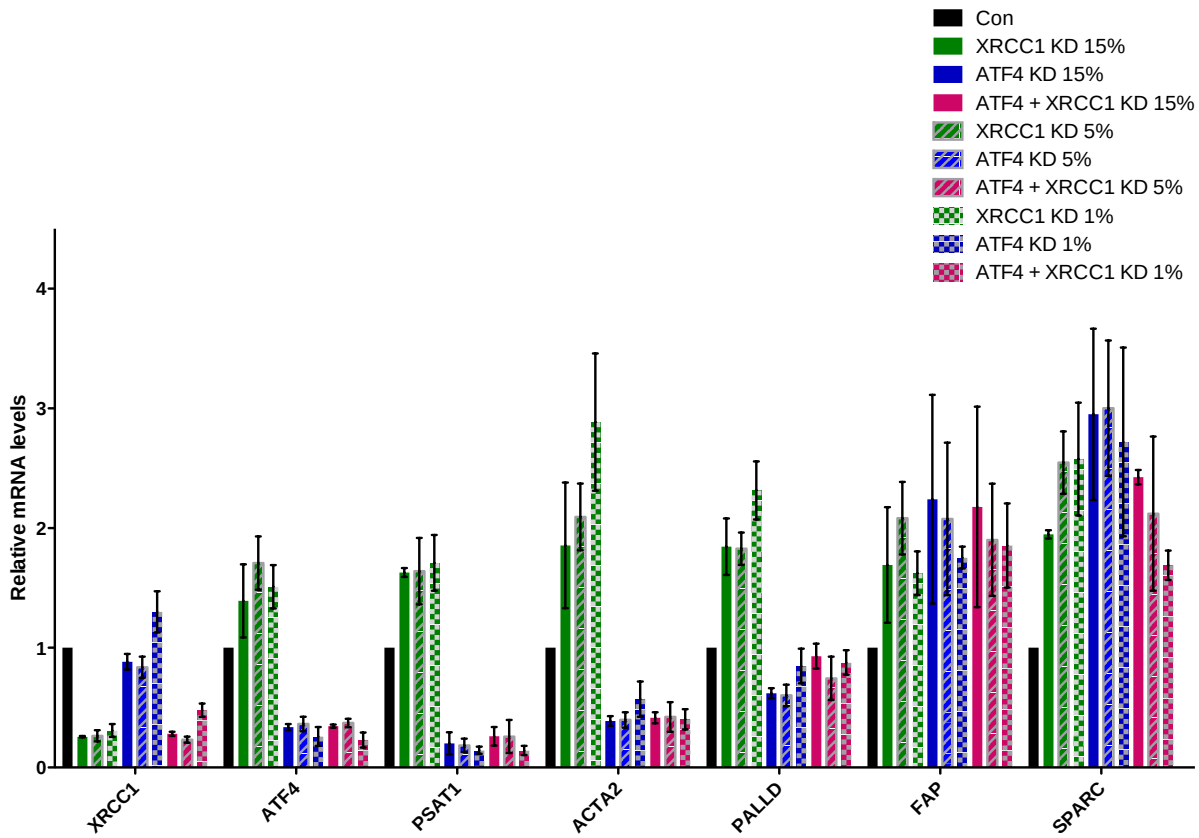

Figure 7: Validation of siRNA-mediated KD of XRCC1 and ATF4 in TIG-1 human fibroblasts grown in different FCS conditions. mRNA levels of indicated genes in TIG-1 fibroblasts transfected with either a non-targeting control siRNA (siCtrl), or siRNAs targeting XRCC1, ATF4, or both grown in different FCS conditions were analysed by RT-qPCR and normalised to GAPDH and B2M and with the respective control treatment set to 1. Data are presented as mean ±SEM. n = 2 for 15%, and n = 4 for 5% and 1%, respectively.

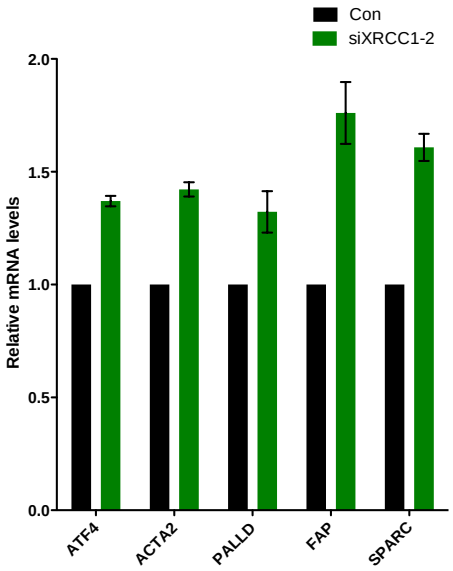

Figure 8: Validation of siXRCC1-mediated transcriptional changes with a second siRNA sequence against XRCC1. mRNA levels of indicated genes in TIG-1 fibroblasts transfected with either a non-targeting control siRNA or siRNA XRCC1-2, grown in 15% FCS were analysed by RT-qPCR and normalised to GAPDH and B2M and with the control treatment set to 1. Data are presented as mean ±SEM. n = 5.

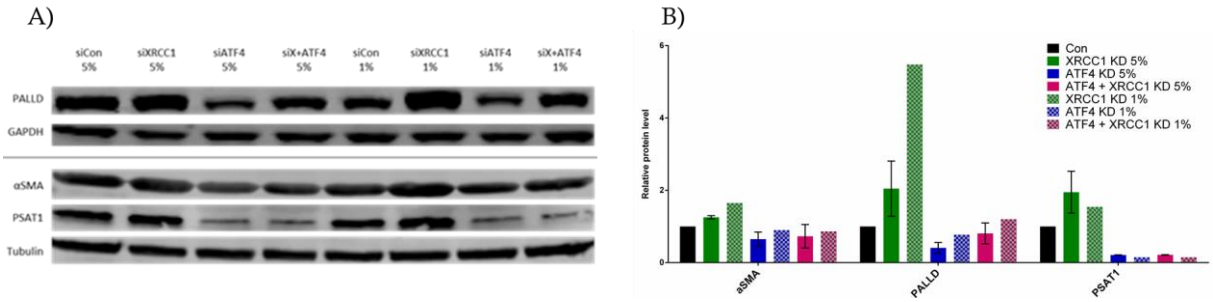

Figure 9: Validation of XRCC1 KD-mediated ATF4-dependent protein expression changes by Western blot analysis of TIG-1 grown under different FCS conditions. A) Western blot analysis of Palladin, aSMA and PSAT1. GAPDH or Tubulin served as loading control. B) Quantification of protein levels as seen in A). Values are mean ± SD from 2 independent experiments for 5% and 1 experiment for 1%, normalised to the loading control, with the control of the respective condition set to 1.

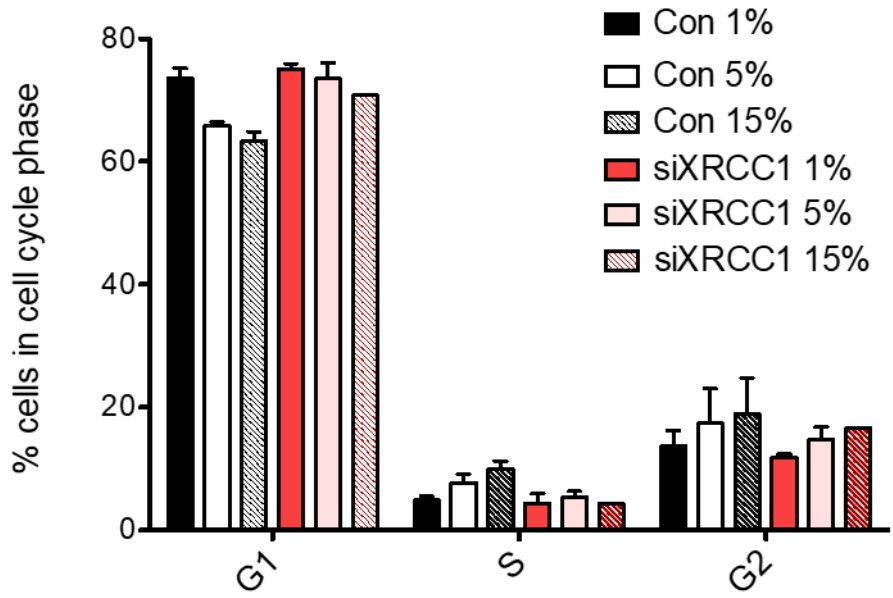

Figure 10: XRCC1 KD cells do not proliferate more than control cells under low FCS conditions. Cell-cycle distribution analysis by flow cytometry of control and XRCC1 KD TIG-1 cells. Shown is the percentage of cells in the respective cell cycle phases. Data are mean ±SD of 2 independent experiments.

6.2 Identification of gene-expression changes in cancer-associated stroma from control and conditional XRCC1 KO mice

6.2.1 Establishment of tissue homogenisation process for mRNA isolation

To identify the best procedure to homogenise fresh-frozen tissue prior to mRNA isolation, four 10 µm sections of the same fresh frozen mouse skin sample mounted on conventional glass slides were used. The sections were scraped off the slides as whole and put in 1.5 ml microcentrifuge tubes (Eppendorf® Safe-Lock Tubes). Then tissue homogenisation was performed using either three different durations of sonication with Covaris® E220 Focused-ultrasonicator, or no sonication but just vortexing for tissue homogenisation, respectively (Table 5). The extracted mRNA was then analysed to obtain RINe values as well as concentration of the samples (Table 5). Procedure D1 (no sonication, repeated vortexing) showed the best RINe value and an appropriate concentration of mRNA (Table 5). As it was also the easiest method without need of any special equipment, D1 was considered the best method for tissue homogenisation for this purpose.

Condition	Homogenisation treatment	**RINe**	**Concentration [pg/µl]**
A1	1 min sonication (Covaris® E220 Focused-ultrasonicator)	2.4	26500
B1	3 min sonication (Covaris® E220 Focused-ultrasonicator)	1.9	5990
C1	5 min sonication (Covaris® E220 Focused-ultrasonicator)	1.7	11500
D1	Repeated vortexing for 5 min	2.5	10800

Table 5: Tissue homogenisation techniques tested for RNA isolation from fresh-frozen tissue with respective RINe values and RNA yields.

To verify this result and test an additional way of sonication, a second trial was performed with three more sections of the same mouse skin tissue comparing sonication using the Bioruptor® plus with vortexing only. Again, vortexing the sample proved to be the simplest method and also yielded the highest amount of mRNA (Table 6). Thus, for further experiments, the vortexing protocol was used for tissue homogenisation.

Condition	**Homogenisation treatment**	**Concentration [pg/µl]**
S 1	1 min of sonication (Bioruptor® plus)	4.5 ng/µl
S 2	3 cycles of sonication (3 x 30 sec on, 30 sec off) (Bioruptor® plus)	5.5 ng/µl
S 3	Vortexing repeatedly for 5 min	5.9 ng/µl

Table 6: List of samples and mRNA yield after mRNA isolation trial using Bioruptor® plus or vortexing

6.2.2 Isolation of tumour-associated and normal stroma from mouse samples

Selective isolation of CAS from control and KO animals (sample number 1 to 7 listed in Table 7) was performed by LCM. The suitable areas were chosen with advice from a pathologist. In general, not much stroma could be found inside the tumour, so stroma from the borders was taken (e.g. Figure 11 A). If available, also stroma from within the tumour was taken (Figure 11 B and C). Normal stroma from unaffected skin was isolated from Samples 8 to 15 listed in Table 7 using LCM (See Figure 12 for examples of selective isolation). To validate the isolation of the chosen tissue parts, the CapSure® Cap and the processed tissue were checked after excision, and pictures were taken to track progress during the entire procedure (examples in Figure 11 and Figure 12). RNA was isolated from CAS and normal stroma from all these cases, and the RINe values and quantity determined (Table 7).

Sample #	Mouse ID	Categorisation	Sample type	RINe	Concentration [pg/ul]
1	SM6026RR	Control	Primary tumour	4.8	638
2	SM6030L	Control	Primary tumour	5.7	959
3	SM6025LL	Control	Primary tumour	-	471
4	SM6029R	Control	Primary tumour	-	736
5	SM6077L	KO	Primary tumour	4.9	592
6	SM6067LR	KO	Primary tumour	3.9	2380
7	SM4962L	KO	Primary tumour	-	598
8	SM6025LL	Control	Skin	4.2	585
9	SM6030L	Control	Skin	5.3	643
10	SM6027LR	Control	Skin	3.7	675
11	SM9173R	Control	Skin	8.5	475
12	SM6077L	KO	Skin	4.9	741
13	SM6067LR	KO	Skin	2.8	681
14	SM9840R	KO	Skin	3.9	1020
15	SM9172RR	KO	Skin	-	104

Table 7: Sample description of the selected tissue for analysis, and concentration and quality of isolated mRNA.

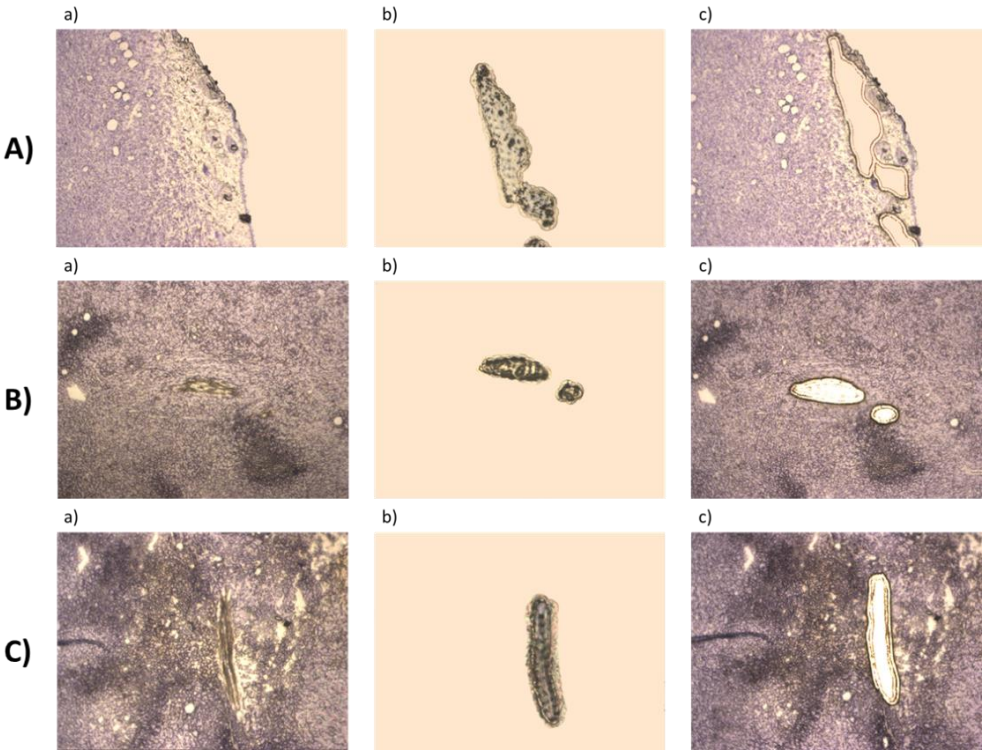

Figure 11: Visual validation of the excised cancer-associated stroma with Laser-capture microdissection from mouse primary tumours at 10x magnification. **a)** native tissue **b**) excised stroma on the CapSure® Cap **c)** tissue after microdissection. **A) S**M6030L (Case 2) **B) & C)** SM6077L (Case 5)

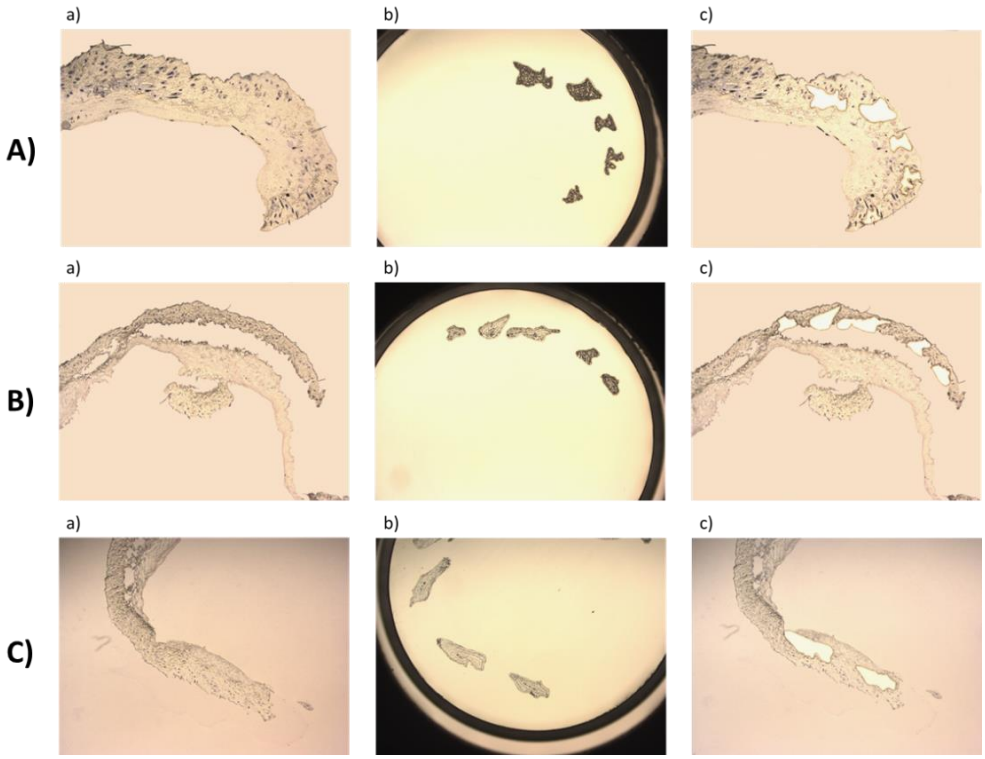

Figure 12: Visual validation of the excised normal stroma with laser-capture microdissection from mouse skin at 2x magnification. **a)** native tissue **b)** excised stroma on the CapSure® Cap **c)** tissue after microdissection. **A)** SM8940R (Case 14) **B) & C)** SM9172RR (Case 15)

6.2.3 Analysis of gene expression in cancer-associated and normal stroma from control and KO animals

To identify gene expression changes between CAS and normal stroma isolated from control and XRCC1 KO mice, the extracted RNA was analysed by NGS. Unsupervised hierarchical clustering of all samples was performed to compare the gene expression in CAS from control and KO animals (Figure 13), as well as in normal skin from control and KO mice (Figure 16). Several samples were excluded due to insufficient performance in NGS.

The main focus of this investigation was laid on identifying differences in gene expression in CAS between KO and control animals. With a significance threshold of $p \leq 0.01$ and log2 fold change threshold of ≥ 0.5, comparing CAS from KO over CAS from control animal, 473 differently expressed genes were identified. Of these, 77 genes were up-regulated and 396 down-regulated in CAS of KO animals. Gene ontology analysis of the deregulated genes identified six clusters (as indicated by the colours on the Y-axis in Figure 13). The biological processes identified within these clusters were the following: the green cluster (cluster 1) contained genes involved in cell adhesion; the yellow cluster (cluster 2), the light blue cluster (cluster 3) and the blue cluster (cluster 4) genes involved in peptide cross-linking and epidermis development; the orange cluster (cluster 5) contained as well genes involved in skin development and genes involved in steroid biosynthetic process; the red cluster (cluster 6) displayed genes involved in steroid hormone mediated signaling pathway (Figure 14). Gene ontology enrichment data for Molecular Functions identified the following main categories (Figure 15): cluster 1 contained genes involved in integrin binding; genes involved in structural molecule activity were found in cluster 2, 3 and 4; in addition, cluster 2 contained genes involved in structural constituent of epidermis, transition metal ion binding, calcium ion binding and cell adhesion molecule binding; genes corresponding to structural constituent of cytoskeleton were found in cluster 3 and 4. For Cellular Compartments the following main categories were identified: in cluster 1 genes assigned to extracellular region, extracellular space, extracellular matrix and collagen trimer were found; cluster 2, 3 and 4 contained genes out of the category cornified envelope; other categories identified for cluster 2 were extracellular exosome, cell junction, intermediate filament cytoskeleton, intermediate filament and keratin filament; additional, in cluster 4 genes corresponding brush border membrane were found (Figure 15). For a more detailed insight, the top 50 up-and down-regulated genes and their association with the respective GO clusters are listed in Table 8 (genes up-regulated in XRCC1 KO CAS) and Table 9 (genes down-regulated in XRCC1 KO CAS).

Taken together, NGS analysis revealed clear differences in CAS and normal stroma from XRCC1-KO compared to control mice. Preliminary analyses suggest that observed changes are consistent with changes in stromal cell biology. A more thorough analysis of these data has the potential to reveal the mechanisms underlying the observed increase of tumour growth and metastasis brought about by a stromal deletion of XRCC1.

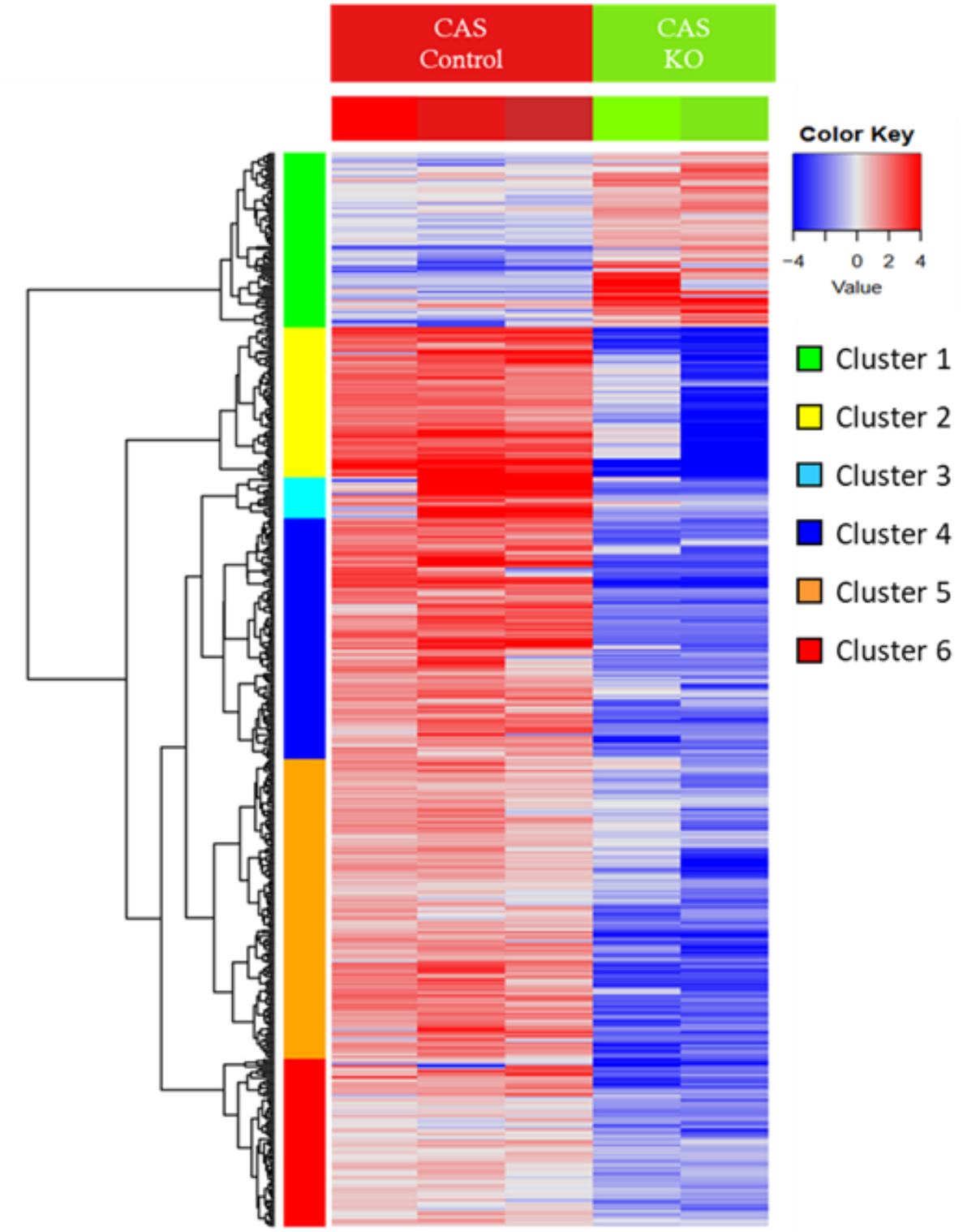

Figure 13: Hierarchical clustering and heatmap of CAS isolated from control and KO mice analysed by NGS ($p \leq 0.01$, log2 ratio threshold of 0.5). 3 samples of CAS from control animals on the left side, and the two samples from KO animals cluster, respectively. Each row features one gene, and each column represents one sample. Gene expression is indicated by the Color Key, red for a relative up-regulation, blue for a relative down-regulation. The bars on the left Y-axis indicate GO clusters associated with the expression patterns.

Biological Processes

Cluster 1 (green)

	Term	ID	p
1	Cell adhesion	GO:0007155	7.53e-7

Cluster 4 (blue)

	Term	ID	p
1	Peptide cross-linking	GO:0018149	2.300927e-10
2	Epidermis development	GO:0008544	4.494916e-09

Cluster 2 (yellow)

	Term	ID	P
1	Peptide cross-linking	GO:0018149	1.594591e-10
2	Skin development	GO:0043588	1.960071e-08
3	Keratinocyte differentiation	GO:0030216	3.899819e-12
4	Keratinization	GO:0031424	1.923647e-10
5	Establishment of skin barrier	GO:0061436	3.699193e-05
6	Epidermis development	GO:0008544	8.424165e-08
7	Cell-cell adhesion	GO:0098609	2.731668e-06

Cluster 5 (orange)

	Term	ID	p
1	Skin development	GO:0043588	2.766689e-06
2	Keratinocyte development	GO:0003334	7.982919e-05
3	Hair follicle development	GO:0001942	2.694217e-05
4	Steroid biosynthetic process	GO:0006694	3.433659e-05
5	Sterol biosynthetic process	GO:0016126	7.800832e-05

Cluster 3 (light blue)

	Term	ID	p
1	Peptide cross-linking	GO:0018149	4.411036e-20
2	Epidermis development	GO:0008544	4.720597e-16

Cluster 6 (red)

	Term	ID	p
1	Steroid hormone mediated signaling pathway	GO:0043401	7.71956e-05

Figure 14: Biological Processes identified through gene ontology enrichment for each cluster. Term = affected biological process, ID = Gene ontology accession number, p = p-value indicating the significance of overlap between biological process and the cancer associated stroma.

Molecular Functions

Cluster 1 (green)			
	Term	ID	p
1	Integrin binding	GO:0005178	4.486012e-05

Cluster 2 (yellow)			
	Term	ID	p
1	Structural molecule activity	GO:0005198	8.134328e-17
2	Structural constituent of epidermis	GO:0030280	2.499800e-10
3	Transition metal ion binding	GO:0046914	7.591503e-06
4	Calcium ion binding	GO:0005509	2.106012e-05
5	Cell adhesion molecule binding	GO:0050839	4.254855e-05

Cluster 3 (light blue)			
	Term	ID	p
1	Structural molecule activity	GO:0005198	2.373627e-08
2	Structural constituent of cytoskeleton	GO:0005200	9.469245e-05

Cluster 4 (blue)			
	Term	ID	p
1	Structural molecule activity	GO:0005198	4.543174e-17
2	Structural constituent of cytoskeleton	GO:0005200	9.078909e-07

Cellular Compartments

Cluster 1 (green)			
	Term	ID	p
1	Extracellular region	GO:0005576	6.966156e-21
2	Extracellular space	GO:0005615	3.648657e-15
3	Extracellular matrix	GO:0031012	1.361759e-18
4	Collagen trimer	GO:0005581	3.085869e-08

Cluster 2 (yellow)			
	Term	ID	p
1	Cornified envelope	GO:0001533	9.513027e-16
2	Extracellular exosome	GO:0070062	3.731239e-08
3	Cell junction	GO:0046914	6.513966e-06
4	Intermediate filament cytoskeleton	GO:0045111	2.453764e-05
5	Intermediate filament	GO:0005882	1.404793e-12
6	Keratin filament	GO:0045095	2.324038e-08

Cluster 3 (light blue)			
	Term	ID	p
1	Cornified envelope	GO:0001533	1.0623e-19

Cluster 4 (blue)			
	Term	ID	p
1	Cornified envelope	GO:0001533	2.801373e-15
2	Brush border membrane	GO:0031526	9.781381e-05

Figure 15: Molecular Functions (left) and Cellular Compartments (right) identified through gene ontology enrichment for the displayed clusters. Term = affected biological process, ID = Gene ontology accession number, p = p-value indicating the significance of overlap between biological process and the cancer associated stroma.

Gene Name	log2 Ratio	pValue	C 1	C 2	C 3	C 4	C 5	C 6
AC174678.2	6.07	7.98e-7						
Sfrp5	5.99	0.0000148	x					
Lats2	5.31	0.000767						
Gbp2b	4.99	0.0002						
Gm28539	4.68	0.000392						
Thbs4	4.53	0.0000109	x	x				
Shh	4.48	0.00365	x	x			x	
Gdf10	4.21	0.00157	x					
Gm38284	4.16	0.00911						
Gm20547	4.07	0.0041	x					
Gm43738	4.07	0.00773						
Nov	4.04	3.36e-7	x					
Bcl2a1a	3.99	0.00882						
Col8a1	3.96	0.00000409	x					
C1ql3	3.95	0.0061	x					
AC154482.1	3.91	0.00458						
Adamts18	3.72	0.00474						
A630073D07Rik	3.65	0.00769						
Myh3	3.65	0.0108						
Cemip	3.58	0.00000878	x					
Col28a1	2.96	0.00563	x					
Disp2	2.93	0.01						
Piezo2	2.9	0.000416						
Prkg2	2.8	0.000185						
Cpxm2	2.7	0.00000972	x					
Cxcl9	2.67	0.00426	x					
Entpd3	2.53	0.009	x					
Mgp	2.49	0.00214	x	x				
Mpz	2.28	0.00444						
Mfap5	2.27	0.00256	x					
Col11a1	2.15	0.00627	x					
Nr2f2	2.14	0.000565						x
C1qtnf3	2.14	0.00314	x					
Arhgap22	2.07	0.000846						
Ccl21a	2.05	0.0106						
Gpc3	2.02	0.0061	x					
Adamtsl3	2.01	0.00473	x					
Col14a1	1.93	0.00644	x					
Lrrc17	1.92	0.00391	x					
Vcam1	1.89	0.00532	x	x				
Ogn	1.85	0.0017	x					
Cxxc5	1.83	0.0109						
Hist1h3i	1.8	0.00832						
Pde7b	1.76	0.00409						
Cybb	1.71	0.000994						
Ptprb	1.7	0.00309						
Apod	1.68	0.00697	x					
Cp	1.62	0.00283	x					
C2	1.61	0.00561	x					
Tnfaip2	1.6	0.00038						

Table 8: List of top 50 up-regulated genes in CAS from XRCC1 KO mice found by NGS. The association of the genes with the 6 identified GO clusters, represented by the coloured columns, is indicated with an x in the respective column.

Gene Name	log2 Ratio	pValue	C 1	C 2	C 3	C 4	C 5	C 6
Lor	-10.00	3.28e-10		x	x	x		
Flg	-10.00	8.33e-8		x	x	x		
Hrnr	-9.63	2.43e-9		x	x	x		
Krt1	-9.32	2.87e-7	x	x	x	x		
Krt77	-8.99	3.93e-8		x	x	x		
Calm4	-8.83	1.26e-9		x				
Flg2	-8.32	6.2e-8		x				
Fam25c	-7.96	4.5e-10						
Dsc1	-7.84	6.32e-11	x	x				
Krt10	-7.46	5.61e-7	x	x	x	x		
Kprp	-7.45	2.62e-9						
Krt6b	-7.45	0.00244		x	x	x		
2310046K23Rik	-7.42	0.00000337		x	x	x		
2310050C09Rik	-7.31	2.91e-9						
Nccrp1	-7.11	9.31e-9	x					
Krtdap	-7.08	1.84e-9	x					
Dsg1a	-6.96	9.63e-7	x	x				
Ivl	-6.91	2.86e-8		x	x	x		
Lce1e	-6.77	0.00000514		x	x	x		
Lce1m	-6.72	3.17e-8		x	x	x		
Lce1f	-6.69	0.0000166		x	x	x		
Lce1h	-6.63	0.00		x	x	x		
Krt16	-6.6	0.00175		x	x	x		
Lce1c	-6.58	6.86e-7		x	x	x		
Lce1i	-6.57	0.00000158		x	x	x		
Lce1j	-6.50	0.0000178		x	x	x		
Cgn	-6.48	2.07e-8						
Krt78	-6.44	4.12e-7	x	x	x	x		
Sprr1b	-6.43	0.00000638		x	x	x		
Lce1g	-6.33	0.0000686		x	x	x		
Sprr2a2	-6.30	0.000121		x	x	x		
Rptn	-6.28	0.00000188	x	x	x	x		
Il1f5	-6.27	1.54e-7	x					
Cnfn	-6.21	3.86e-7		x	x	x		
Lce1d	-6.19	0.00000287		x	x	x		
Pla2g4f	-6.10	7.97e-7		x				
Pla2g2f	-6.09	0.00000155	x					
Ly6d	-6.07	2.1e-7						
Lce1a1	-6.05	0.00000378		x	x	x		
Sprr2a1	-6.05	0.000816		x	x	x		
Ppfia3	-6.01	4.42e-7						
Mapk13	-5.91	0.00000119						
Casp14	-5.9	7.06e-7	x					
Gsdma	-5.77	0.0000132						
Cdcp1	-5.73	0.00000322						
Exph5	-5.72	0.00000592						
Fgfbp1	-5.70	0.0000129	x					
Lce1a2	-5.68	0.00000492		x	x	x		
Angptl7	-5.68	0.0000873	x					
BC100530	-5.65	0.000986						

Table 9: List of top 50 down-regulated genes in CAS from XRCC1 KO mice found by NGS. The association of the genes with the 6 identified GO clusters, represented by the coloured columns, is indicated with an x in the respective column.

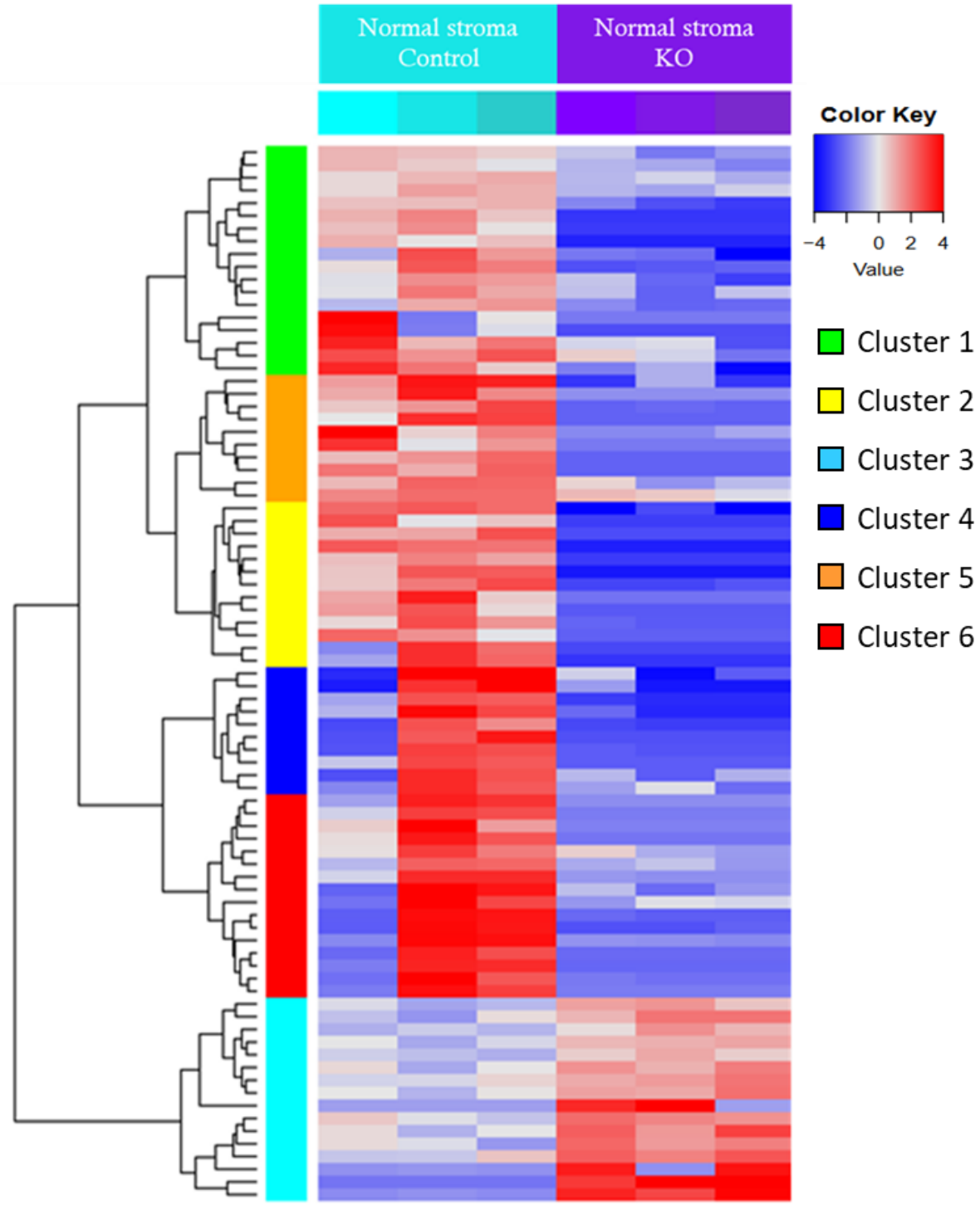

Figure 16: Hierarchical clustering and heatmap of normal stroma isolated from control and KO mice analysed by NGS ($p \leq 0.01$, log2 ratio threshold of 0.5). The 3 samples of normal stroma isolated from control animals, and the 3 samples of normal stroma from KO animals cluster, respectively. Each row features one gene, and each column represents one sample. Gene expression is indicated by the Color Key, red for a relative up-regulation, blue for a relative down-regulation. The bars on the left side indicate clusters associated with the respective expression patterns (legend on the right side).

Top 20 up-regulated genes

Gene name	log2 Ratio	pValue
1700047I17Rik2	7.62	0.00000778
Gm38215	4.93	0.000409
Gm6563	4.45	0.00798
Tbx6	4.43	0.00918
Hmga1b	4.35	0.0104
Hist1h2ah	4.27	0.0131
Gm43178	4.24	0.0155
Ugt1a6b	4.11	0.0306
Olfr648	4.03	0.015
Dnah10	3.88	0.0322
Rpl9-ps6	3.77	0.042
Nwd1	3.76	0.0352
Gm45416	3.67	0.0279
4930405N21Rik	3.56	0.0258
Fgf9	3.51	0.0369
Cfap157	3.49	0.0246
Cib3	3.46	0.0266
Mterf1b	3.45	0.0238
Gm10130	3.35	0.0286
Cacna2d4	3.27	0.0291

Top 20 down-regulated genes

Gene name	log2 Ratio	pValue
Fam177a	-6	0.000804
Has1	-5.9	0.0061
Skint5	-5.65	0.007
Pou3f1	-5.64	0.00211
Spint1	-5.59	0.00166
Mvk	-5.54	0.000138
Dusp5	-5.53	0.0000836
Cgn	-5.49	0.00694
2310050C09Rik	-5.44	0.00797
Lce1m	-5.44	0.0205
Them5	-5.36	0.00301
Ereg	-5.26	0.000805
Lce1a2	-5.11	0.00505
Dab1	-5.1	0.00476
Cpa4	-5.05	0.00159
Xirp1	-5.04	0.0102
Prob1	-5.01	0.00542
Hist1h2bf	-4.88	0.0022
Crct1	-4.86	0.00332
Igha	-4.82	0.00428

Table 10: List of top 20 up-regulated (left) and down-regulated (right) genes found by RNA sequencing comparing normal, unaffected skin from XRCC1 KO and control mice.

7 Discussion

Nowadays, cancer plays a huge role in our health care system. Globally, about 1 in 6 deaths occurs due to cancer (https://www.who.int/en/news-room/fact-sheets/detail/cancer), despite ongoing research for novel ways of diagnosis and therapy. Recent findings have shown, that cancer cells do not manifest the disease alone but strongly depend on their surrounding stroma, the CAS. Thus, targeting CAS is regarded as a promising approach for the development of new cancer treatments [4, 5]. One prominent component within CAS are the CAFs, which have been shown to support tumour growth and metastasis, and are a major factor in determining the tumour outcome [7].
It is already known, that CAF formation can be induced *in vitro* by inflammatory cytokines, such as TGF β and/or ROS [8, 9], but the molecular mechanisms underlying this transformation remains unclear. Our group has recently demonstrated that exposure to these agents results in a depletion of XRCC1, which causes persistent DNA damage, that in turn leads to activation of CAFs that support growth and motility of tumour cells *in vitro*. This reprogramming, which can also be observed upon XRCC1 KD in fibroblasts, partly depends on the integrative stress response through upregulation of ATF4 which seems to induce a metabolic rewiring that might increase nutritional self-sufficiency ([10, 14] and unpublished data). But the reason for this reprogramming through XRCC1 downregulation remains enigmatic. The available data led us to hypothesise that XRCC1 KD cells might survive better in a 'nutrient-starved' environment. By analysing TIG-1 fibroblasts grown under nutrient-restricted conditions, we found that XRCC1 KD cells, which show a CAF-like phenotype, truly have a growth and/or survival advantage over control cells. Additionally, by knocking down ATF4 together with XRCC1, we demonstrated that this advantage depends on ATF4 (Figure 6). An analysis of the cell cycle revealed that XRCC1 KD cells did not proliferate more than control cells, suggesting that their advantage at nutrient-starved conditions is likely due to an increased resistance to apoptosis (Figure 10).
Furthermore, data from our lab demonstrated that a stromal XRCC1 knockout (KO) triggers increased tumour growth and metastasis *in vivo* (unpublished data). To understand what molecular changes in the stroma of XRCC1 KO mice could be the underlying cause for this phenotype, we analysed the molecular changes in CAS from control and XRCC1 KO mice by laser-capture microdissection coupled with NGS. By doing so, we found differences in gene expression between the two groups, which presumably are connected to the increased tumour growth and metastasis and will allow further, more detailed analysis (Figure 13, Figure 14, Figure 15).

7.1 Identification of an ATF4-dependent survival advantage of XRCC1 KD cells under low-serum condition

By seeding the same number of TIG-1 fibroblasts, transfected with either siXRCC1 or a control siRNA, grow in medium containing different concentrations of FCS (15%, 5% or 1%), we were able to show that, with a decreasing amount of serum, the XRCC1 KD cells showed increased density and less rounded, floating cells compared to the control cells (Figure 6). This demonstrated that XRCC1 KD cells are more viable under starved conditions. To verify that the KD capacity of the siRNAs was not affected by the low-FCS condition, RT-qPCR and Western blot were performed, analysing the direct target of the siRNA and also several respective downstream targets. However, to get the samples for this validation was quite challenging. We were facing the problem, that in the 1% FCS condition the number of control, siATF4 and combined siATF4 and XRCC1 KD cells all were considerably lower than the

number of XRCC1 KD cells on the day of cell collection, making it difficult to extract sufficient mRNA or protein for downstream analysis. To improve the cell numbers, we tried to start with more cells, by seeding more cells for the siRNA treatment, and subsequently splitting 2/3 of these cells into the 1% FCS condition. However, contrary to expectations, this approach failed and even aggravated the outcome. Most of the control cells were detached and floating, while XRCC1 KD cells were still perfectly viable and formed a dense cell layer. This led us to the conclusion, that with a higher number of cells the already sparse FCS was used up even faster, and thus all except XRCC1 KD cells were starving to death. This result further supported the hypothesis that XRCC1-depleted TIG-1 fibroblasts have an advantage in nutrient-restricted conditions due to an ATF4 mediated metabolic reprogramming which in turn seem to support nutritional self-sufficiency (unpublished observations). The finding that a decline in BER capacity confers fibroblasts with an increased resilience towards nutrient starvation is very interesting from several points of view. We have previously demonstrated that lengthened exposure to pro-inflammatory cytokines and ROS, both of which are widely accepted as inducers of CAF activation, induce a deficiency in BER through transcriptional down-regulation of XRCC1 and lead to persistent DNA damage, suggesting a link between XRCC1 downregulation and CAF activation [14]. Indeed, CAF activation can be achieved directly by XRCC1 KD without exposure to cytokines or ROS, suggesting that persistent DNA damage is an integral part of the CAF activation mechanism [14]. Mechanistically, persistent DNA damage signalling by ATM has been shown to phosphorylate the transcription factor Sp1, thus initiating its degradation [32]. As Sp1 in turn controls expression of XRCC1, degradation of Sp1 leads to a suppression of XRCC1 transcription, thus triggering a decline in BER capacity and further aggravating the persistent DNA damage. A very similar mechanism might be involved in reading to XRCC1 downregulation upon exposure to TGF β or ROS, and suggests BER downregulation in fibroblasts to be a general response to stressful events. But the question why the cell would initiate such a BER decline under stressful conditions has remained elusive until now. It has been suggested, that such cells might undergo apoptosis more easily or be eliminated better by the immune system [32]. However, human fibroblasts have been shown to be highly resistant to apoptosis, and undergo senescence much rather than inducing apoptosis, and can be maintained in culture for extremely long periods in that state [33]. This is in line with the crucial role of fibroblasts to maintain the organism's structural integrity, because, even in a post-replicative senescent state, fibroblasts are still able to actively shape the extracellular matrix. This would not be possible were damaged fibroblasts quickly eliminated through apoptosis or by the immune system. Additionally, yet unpublished data from our lab reveals wide-ranging metabolic reprogramming of fibroblasts in which BER capacity is depleted by XRCC1 KD. These changes potentially increase cellular self-sufficiency with respect to many metabolites, such as nucleotides, amino acids and energy. Our finding showing that fibroblasts experiencing persistent DNA damage have a survival advantage under nutrient-starved conditions further support the functionality of this metabolic reprogramming. Thus, we propose that under stressful circumstances, such as protracted inflammation or persistent signalling from tumour cells, DNA damage is induced in the tissue-resident fibroblasts, which leads to ATM-signalling that in turn destabilizes the transcription factor Sp1. This causes XRCC1 transcription to decrease, resulting in a BER-depleted cellular state that further aggravates persistence of DNA damage. This initiates ATF4-dependent metabolic reprogramming that increases cellular self-sufficiency in nutrients, thus enabling these cells to survive even in nutrient-starved conditions. Through this increased resilience, fibroblasts can still fulfil their important structural roles in the organism, as they are the main responsible for synthesis of the extracellular matrix, that provides the structural scaffold for other cells to grow on and mechanical properties that determine the integrity of

organs [34]. Such a resilience mechanism seems important especially also for CAFs. *Per definitionem*, CAFs are located closely adjacent to the epithelial tumour-forming, rapidly dividing cancer cells. These cancer cells have a huge demand in a wide variety of nutrients to sustain their high proliferative rate, and they have been shown to remodel the surrounding stroma in a way that increases the delivery of such nutrients and other growth-promoting molecules [5]. Specifically, CAFs have been found to take up metabolic waste of cancer cells to produce metabolites that in turn are secreted again to feed the tumour [18]. It is thus thought that most of the 'rich' nutrients are drained away from CAFs to support tumour growth, which results in the necessity for CAFs to survive in a 'starved' environment. The observed down-regulation of BER capacity in fibroblasts exposed to a maintained pro-inflammatory stimulation that induces CAF generation seems to thus increase self-sufficiency of these cells, which would be beneficial in a starved environment. In summary, our observations suggest the metabolic rewiring upon BER decline after stressful insults to be a physiological response of fibroblasts to ensure their survival in nutrient-starved conditions, in order to fulfil their principal role of maintaining the structure of the organism.

ATF4 is a transcription factor that has a dual role in cells promoting either their adaptation to endure stress or the induction of apoptosis [35]. Furthermore, an indirect influence of ATF4 on cell viability modulating the balance of anabolic and catabolic processes has been suggested. ATF4 activates transcription of a set of targets involved in autophagy, but also targets that upregulate protein synthesis. This whole process is quite complex and bimodal, in a way that at the end it can have either pro- or anti-apoptotic effects, likely depending on the balance between anabolism and catabolism. This balance is also context-dependent, as for example autophagy can become damaging when the amount of expendable proteins is exhausted and the cell is not able to compensate for the loss. Thus, highly proliferative cells might be more resistant to autophagy, as they have high levels of protein synthesis and ER load. Moreover, it has been suggested that cancer cells might be more resistant to pro-apoptotic ATF4 targets, because they already have defects in apoptotic signalling downstream of ATF4 [35]. The ATF4-dependence of the metabolic reprogramming that we observed upon XRCC1 is nicely in line with our previous findings demonstrating ATF4 induction after XRCC1 KD [10] as well as its involvement in the transcription of several CAF-markers that are activated upon XRCC1 KD [14]. It also raises several more intriguing questions. Firstly, it will be of interest to determine which are the exact ATF4-dependent changes that allow cells to thrive in nutrient-starved conditions. Thus far unpublished results from our lab show wide-ranging changes in metabolic processes involving synthesis of nucleotides and amino acids and the production of energy, some or all of which could be involved in this. Furthermore, our results suggest that rather than having a proliferative advantage, XRCC1 KD cells are more resistant to apoptosis in nutrient-starved conditions which confers them a survival advantage that results in higher cell density. Hence, XRCC1 KD cells seem somehow to be able to exploit ATF4, similarly to cancer cells, to reduce stress resulting from nutrient limitation and benefit from its pro-survival effects. The increased resistance of XRCC1 KD cells to apoptosis should further be verified by i) measuring amounts of apoptotic cells when grown at 1% FCS, ii) investigating the propensity to undergo apoptosis upon stimulation with known apoptosis-inducing agents, iii) analyse the activation status of ATF4-dependent apoptotic and pro-survival signalling pathways, iv) demonstrate by loss-of-function and gain-of-function experiments which signalling circuitries are mediating the observed resistance to apoptosis. A deeper understanding of these mechanisms might also facilitate the identification of pharmacological targets to target CAS, which is currently viewed as a promising strategy for cancer treatment [4, 36-40].

7.2 Identification of gene-expression changes in cancer-associated stroma from control and conditional XRCC1 KO mice

7.2.1 Mouse model and sample preparation

To analyse the impact of XRCC1 KO on tumour growth and metastasis *in vivo*, it was necessary to employ a conditional KO strategy, because a full KO of XRCC1 is embryonically lethal [15, 16]. With our model using the Col1a2-Cre approach, it was possible to restrict the KO largely to fibroblasts [41]. Additionally, the inducibility by Tamoxifen added another layer of control, making it possible to induce the KO after weaning by Tamoxifen administration, therefore circumventing possible developmental defects. Thus, we generated apparently healthy mice without any overt phenotypic differences between KO and control animals. The mouse model was already established in the Markkanen lab before my project started and the animals were in breeding.
As tumour model to analyse the effect of the stroma on tumour growth and metastasis, Lewis Lung Carcinoma (LLC) cells were chosen for injection for several reasons. Since LLCs are often used in tumour research, they are well characterised, and primary tumours grow reliably [42]. Importantly, LLCs also show a certain tendency to metastasise, which was important to analyse the effect on metastasis. And finally, since our recipient animals were fully immune-competent, a syngeneic cell line had to be used. For all these reasons, LLCs were the cells of choice.
During surgical tissue excision, fresh-freezing and sample preparation for LCM, we took great care to treat all the samples the same. Nevertheless, there were large variations in the extracted mRNA quality and quantity (Table 7). There are a lot of possible reasons that could explain these differences, ranging from differences in the exact time elapsed between surgical excision and freezing, the preparation of sections and slides, and others. The Institute for Veterinary Pathology Zürich made an effort to cut the samples as soon as possible, but even so they had busy days where the samples then stayed in the freezer at -20°C for a longer time. The probably most important and influential step was presumably the laser microdissection, where the tissue stayed out at room temperature due to the procedure. Some tissues were easy to cut, others needed to be cut several times till it was possible to take the excised part out. Frozen tissue still contains RNases, which become active as the tissue thaws [43]. Therefore, the quicker the microdissection, the better for RNA. Further, there were differences between the samples themselves. Some contained nice areas of stroma without any unwanted cells, in others just very little stroma was found, or it contained lots of glands and hair follicles that made excision more difficult and cumbersome. Nevertheless, suitable amounts of mRNA could be extracted to send for sequencing. During NGS several samples were excluded due to insufficient performance in during the run. Still, enough data was generated to analyse gene expression comparing CAS and normal stroma from control and KO mice.

7.2.2 Gene expression analysis in CAS comparing KO and control mice

Unsupervised hierarchical clustering of CAS from control and KO animals (Figure 13) showed clear differences in gene expression, with a total of 473 deregulated genes in KO compared to control. Results from gene ontology analysis suggest that these differences are likely to be linked to increased tumour growth and metastasis, as for instance cell adhesion is one main category found within the deregulated biological processes in Cluster 1(Figure 14) and integrin binding within the deregulated molecular functions (Figure 15) which are both strongly connected to cancer invasion and metastasis [44]. Other

categories among the deregulated biological processes are connected to steroid biosynthetic processes or steroid hormone mediated signalling pathways (Figure 14, Cluster 5 and 6). This is interesting, for it is known that steroids play a role in cancer development and metastasis [45, 46] [Haslam, 2001, Breast Cancer Res.]. Furthermore, this also suggests that the differences in gene expression found in our experiments are connected to the macroscopic findings of increased tumour growth and metastasis that were observed in these mice. Furthermore, we had a quick scan through the top 50 up- and top 50 down-regulated genes, where several types of collagens were found among the up-regulated targets. Increased collagen deposition and crosslinking is one of the mainstay features of CAS that is secreted by CAFs and supports the invasion of cancer cells [5, 36-40], and an increase in collagen expression has been associated with a higher risk of metastasis in humans [47] and dogs [48]. Importantly also, deregulation of many collagens has been observed repeatedly in our laboratory using the XRCC1 KD fibroblast model *in vitro* (data not shown), which further supports XRCC1 depletion in fibroblasts as the driving force behind the observed changes.
In summary we were able to show that there are molecular changes associated with cancer growth and metastasis in the tumour stroma of mice with a stromal XRCC1 depletion compared to control mice. However, due to lack of time, no detailed analysis was made thus far. Nevertheless, the obtained data is very promising for future investigations.

7.2.3 Gene expression analysis in normal unaffected stroma in KO and control mice

In addition to the comparison on CAS between the two groups of KO and control animals we also extracted mRNA from normal, non-tumour-associated stroma from the same mouse model. The unsupervised hierarchical clustering of normal stroma from control and KO animals reveals much less differentially expressed genes and overall larger variations between the samples of the two groups (Figure 16). Since CAFs are known to strongly interact with and be influenced by cancer cells, less effect was assumed in the absence of this interplay. This possibly explains the absence of huge changes in these samples of normal skin, as here fibroblasts are not interacting with tumour cells. Again, due to time restrictions, there unfortunately was no time for a closer investigation of the data, but it lays a good basis for future research.

7.2.4 Conclusion

To conclude, we come back to the two main questions asked at the beginning:

1. **Does XRCC1 depletion in fibroblasts induce changes that support their survival in restricted growth conditions? If yes, is this dependent on the stress-responsive transcription factor ATF4?**

We have demonstrated that XRCC1 KD cells have a clear survival advantage under nutrient-restricted growth conditions by analysing cell morphology and density. The findings were validated by RT-qPCR and Western blot, showing that the KD was consistent in all the conditions. Furthermore, we were also able to show that these survival advantages depend on the upregulation of ATF4 by a co-knockdown of XRCC1 and ATF4, which resulted in a rescue of the observed phenotype in XRCC1 KD cells.
Taking the investigation a step further by analysing cell cycle phases of control and XRCC1 KD cells grown in 15%, 5% or 1% FCS conditions, we found that the advantage of XRCC1 KD cells is likely due to an increased resistance to apoptosis. Because no increase in S-phase but rather a prolonged G1 phase was discovered in XRCC1 KD cells compared to control. To further support this hypothesis, it will be necessary to address the exact mechanism by which ATF4 imparts survival of XRCC1 KD cells in nutrient-starved conditions. Detailed understanding of the role of ATF4 in CAS has the potential to identify novel therapeutic approaches to target CAS.

2. **What molecular changes can be observed in the tumour stroma of mice with a stromal XRCC1 depletion? How do these changes support tumour growth and metastasis?**

We successfully isolated mRNA from the desired tissue and performed Next-generation Sequencing. From the generated data we see that there are differences in gene-expression between CAS from control and KO mice and less so in normal stroma. Considering that CAFs are known to interact with cancer cells, that were absent in normal tissue, this was not unexpected. Furthermore, a first evaluation of the data suggests that the observed differences in gene expression could well be connected to the observed increase in tumour growth and metastasis. The generated data allows more detailed investigations of the molecular changes found in tumour stroma and as it will also be possible to identify interesting deregulated targets, this could help in understanding how the changes support tumour growth and metastasis.

8 Acknowledgements

Finally, I would like to thank everyone that supported me during my work.
A special thanks goes to my supervisor Enni Markkanen for leading me through this project, always being present as contact person when facing troubles in the lab and helping me with writing.
Furthermore, also a big thank you to Elena Clementi, who introduced me to all the experimental work and lab routines, always patiently listening to my questions and helping me with the interpretation of my results.

I would also like to acknowledge the whole Markkanen and Nägeli group for providing a comfortable working area and being helpful in small questions that occurred, making the time in the lab very enjoyable. Moreover, I would like to thank the Institute of Veterinary Pathology and the Functional Genomics Center for their support.

At last, I would also like to thank my family and friends for being patient and supportive in any situation.

9 References

1. World Health Organization WHO Cancer facts sheet https://www.who.int/en/news-room/fact-sheets/detail/cancer/.

2. Bray F, Ferlay J, Soerjomataram I, et al (2018) Global cancer statistics 2018: GLOBOCAN estimates of incidence and mortality worldwide for 36 cancers in 185 countries. CA Cancer J Clin 68:394–424. doi: 10.1016/S0140-6736(15)00135-X

3. Ferlay J, Colombet M, Soerjomataram I, et al (2018) Cancer incidence and mortality patterns in Europe: Estimates for 40 countries and 25 major cancers in 2018. Eur J Cancer 103:356–387. doi: 10.1016/j.ejca.2018.07.005

4. Valkenburg KC, de Groot AE, Pienta KJ (2018) Targeting the tumour stroma to improve cancer therapy. Nat Rev Clin Oncol 15:366–381. doi: 10.1038/s41571-018-0007-1

5. Hanahan D, Coussens LM (2012) Accessories to the Crime: Functionsof Cells Recruited to the Tumor Microenvironment. Cancer Cell 21:309–322. doi: 10.1016/j.ccr.2012.02.022

6. Li H, Fan X, Houghton J (2007) Tumor microenvironment: the role of the tumor stroma in cancer. J Cell Biochem 101:805–815. doi: 10.1002/jcb.21159

7. Madar S, Goldstein I, Rotter V (2013) "Cancer associated fibroblasts--"more than meets the eye. Trends in Molecular Medicine 19:447–453. doi: 10.1016/j.molmed.2013.05.004

8. Calon A, Tauriello DVF, Batlle E (2014) TGF-beta in CAF-mediated tumor growth and metastasis. Seminars in Cancer Biology 25:15–22. doi: 10.1016/j.semcancer.2013.12.008

9. Costa A, Scholer-Dahirel A, Mechta-Grigoriou F (2014) The role of reactive oxygen species and metabolism on cancer cells and their microenvironment. Seminars in Cancer Biology 25:23–32. doi: 10.1016/j.semcancer.2013.12.007

10. Markkanen E, Fischer R, Ledentcova M, et al (2015) Cells deficient in base-excision repair reveal cancer hallmarks originating from adjustments to genetic instability. Nucleic Acids Research 43:3667–3679. doi: 10.1093/nar/gkv222

11. Nazarkina ZK, Khodyreva SN, Marsin S, et al (2007) XRCC1 interactions with base excision repair DNA intermediates. DNA Repair (Amst) 6:254–264. doi: 10.1016/j.dnarep.2006.10.002

12. Dianov GL, Hübscher U (2013) Mammalian Base Excision Repair: the Forgotten Archangel. Nucleic Acids Research. doi: 10.1093/nar/gkt076

13. Fan J, Wilson PF, Wong H-K, et al (2007) XRCC1 down-regulation in human cells leads to DNA-damaging agent hypersensitivity, elevated sister chromatid exchange, and reduced survival of BRCA2 mutant cells. Environ Mol Mutagen 48:491–500. doi: 10.1002/em.20312

14. Legrand AJ, Poletto M, Pankova D, et al (2018) Persistent DNA strand breaks induce a CAF-like phenotype in normal fibroblasts. Oncotarget. doi: 10.18632/oncotarget.24446

15. Tebbs RS, Flannery ML, Meneses JJ, et al (1999) Requirement for the Xrcc1 DNA base excision repair gene during early mouse development. Dev Biol 208:513–529. doi: 10.1006/dbio.1999.9232

16. Tebbs RS, Thompson LH, Cleaver JE (2003) Rescue of Xrcc1 knockout mouse embryo lethality by transgene-complementation. DNA Repair (Amst) 2:1405–1417.

17. Harding HP, Zhang Y, Zeng H, et al (2003) An integrated stress response regulates amino acid metabolism and resistance to oxidative stress. Mol Cell 11:619–633.

18. Lyssiotis CA, Kimmelman AC (2017) Metabolic Interactions in the Tumor Microenvironment. Trends Cell Biol 27:863–875. doi: 10.1016/j.tcb.2017.06.003

19. Ettlin J (2017) Analysis of Gene Expression Signatures in Cancer-Associated Stroma from Canine Mammary Tumours; Master thesis. Vetsuisse Faculty, University of Zurich

20. Amini P, Ettlin J, Opitz L, et al (2017) An optimised protocol for isolation of RNA from small sections of laser-capture microdissected FFPE tissue amenable for next-generation sequencing. BMC Mol Biol 18:22. doi: 10.1186/s12867-017-0099-7

21. Espina V, Wulfkuhle JD, Calvert VS, et al (2006) Laser-capture microdissection. Nat Protoc 1:586–603. doi: 10.1038/nprot.2006.85

22. Feil S, Valtcheva N, Feil R (2009) Inducible Cre mice. Methods in Molecular biology (Clifton, NJ) 530:343–363. doi: 10.1007/978-1-59745-471-1_18

23. Bolger AM, Lohse M, Usadel B (2014) Trimmomatic: a flexible trimmer for Illumina sequence data. Bioinformatics 30:2114–2120. doi: 10.1093/bioinformatics/btu170

24. Dobin A, Davis CA, Schlesinger F, et al (2013) STAR: ultrafast universal RNA-seq aligner. Bioinformatics 29:15–21. doi: 10.1093/bioinformatics/bts635

25. Bray NL, Pimentel H, Melsted P, Pachter L (2016) Near-optimal probabilistic RNA-seq quantification. Nature Biotechnology 34:525–527. doi: 10.1093/bioinformatics/bts480

26. Robinson MD, McCarthy DJ, Smyth GK (2010) edgeR: a Bioconductor package for differential expression analysis of digital gene expression data. Bioinformatics 26:139–140. doi: 10.1093/bioinformatics/btp616

27. Robinson MD, Oshlack A (2010) A scaling normalization method for differential expression analysis of RNA-seq data. Genome Biology 11:R25. doi: 10.1186/gb-2010-11-3-r25

28. Young MD, Wakefield MJ, Smyth GK, Oshlack A (2010) Gene ontology analysis for RNA-seq: accounting for selection bias. Genome Biology 11:R14. doi: 10.1186/gb-2010-11-2-r14

29. Brem R, Hall J (2005) XRCC1 is required for DNA single-strand break repair in human cells. Nucleic Acids Research 33:2512–2520. doi: 10.1093/nar/gki543

30. Lee HW, Park YM, Lee SJ, et al (2013) Alpha-smooth muscle actin (ACTA2) is required for metastatic potential of human lung adenocarcinoma. Clin Cancer Res 19:5879–5889. doi: 10.1158/1078-0432.CCR-13-1181

31. Gao S, Ge A, Xu S, et al (2017) PSAT1 is regulated by ATF4 and enhances cell proliferation via the GSK3β/β-catenin/cyclin D1 signaling pathway in ER-negative breast cancer. J Exp Clin Cancer Res 36:179. doi: 10.1186/s13046-017-0648-4

32. Fletcher SC, Grou CP, Legrand AJ, et al (2017) Sp1 phosphorylation by ATM downregulates BER and promotes cell elimination in response to persistent DNA damage. Nucleic Acids Research. doi: 10.1093/nar/gkx1291

33. Wang E (1995) Senescent human fibroblasts resist programmed cell death, and failure to suppress bcl2 is involved. Cancer Res 55:2284–2292.

34. Tigges J, Krutmann J, Fritsche E, et al (2014) Mechanisms of Ageing and Development. Mechanisms of Ageing and Development 138:26–44. doi: 10.1016/j.mad.2014.03.004

35. Wortel IMN, van der Meer LT, Kilberg MS, van Leeuwen FN (2017) Surviving Stress: Modulation of ATF4-Mediated Stress Responses in Normal and Malignant Cells. Trends in Endocrinology & Metabolism 28:794–806. doi: 10.1016/j.tem.2017.07.003

36. Gandellini P, Andriani F, Merlino G, et al (2015) Complexity in the tumour microenvironment: Cancer associated fibroblast gene expression patterns identify both common and unique features of tumour-stroma crosstalk across cancer types. Seminars in Cancer Biology. doi: 10.1016/j.semcancer.2015.08.008

37. Luo H, Tu G, Liu Z, Liu M (2015) Cancer-associated fibroblasts: a multifaceted driver of breast cancer progression. CANCER LETTERS 361:155–163. doi: 10.1016/j.canlet.2015.02.018

38. Majidinia M, Yousefi B (2017) Breast tumor stroma: A driving force in the development of resistance to therapies. Chem Biol Drug Des 12:541. doi: 10.1111/cbdd.12893

39. Soysal SD, Tzankov A, Muenst SE (2015) Role of the Tumor Microenvironment in Breast Cancer. Pathobiology 82:142–152. doi: 10.1159/000430499

40. Zhang J, Liu J (2013) Tumor stroma as targets for cancer therapy. Pharmacol Ther 137:200–215. doi: 10.1016/j.pharmthera.2012.10.003

41. Zheng B, Zhang Z, Black CM, et al (2002) Ligand-dependent genetic recombination in fibroblasts : a potentially powerful technique for investigating gene function in fibrosis. Am J Pathol 160:1609–1617. doi: 10.1016/S0002-9440(10)61108-X

42. Zhu H, Kauffman ME, Trush MA, et al (2018) A Simple Bioluminescence Imaging Method for Studying Cancer Cell Growth and Metastasis after Subcutaneous Injection of Lewis Lung Carcinoma Cells in Syngeneic C57BL/6 Mice. React Oxyg Species (Apex) 5:118–125. doi: 10.20455/ros.2018.813

43. Application note MagMax FFPE DNA/RNA ultra kit; https://assets.thermofisher.com/TFS-Assets/BID/Application-Notes/comparison-dna-rna-fresh-frozen-ffpe-app-note.pdf.

44. Gkretsi V, Stylianopoulos T (2018) Cell Adhesion and Matrix Stiffness: Coordinating Cancer Cell Invasion and Metastasis. Front Oncol 8:145. doi: 10.3389/fonc.2018.00145

45. Alferez DG, Simões BM, Howell SJ, Clarke RB (2018) The Role of Steroid Hormones in Breast and Effects on Cancer Stem Cells. Curr Stem Cell Rep 4:81–94. doi: 10.1007/s40778-018-0114-z

46. Haslam SZ, Woodward TL (2001) Reciprocal regulation of extracellular matrix proteins and ovarian steroid activity in the mammary gland. Breast Cancer Res 3:365–372.

47. Takai K, Le A, Weaver VM, Werb Z (2016) Targeting the cancer-associated fibroblasts as a treatment in triple-negative breast cancer. Oncotarget 7:82889–82901. doi: 10.18632/oncotarget.12658

48. Klopfleisch R, Lenze D, Hummel M, Gruber AD (2011) The Veterinary Journal. The Veterinary Journal 190:236–243. doi: 10.1016/j.tvjl.2010.10.018